INTERNATIONAL JOURNAL FOR NUMERICAL METHODS IN ENGINEERING
Int. J. Numer. Meth. Engng 2013; **96**:842–866
Published online 3 September 2013 in Wiley Online Library (wileyonlinelibrary.com). DOI: 10.1002/nme.4564

A direct coupling method for 3D hydroelastic analysis of floating structures

Ki-Tae Kim[1], Phill-Seung Lee[1,*,†] and K. C. Park[1,2]

[1]*Division of Ocean Systems Engineering, Korea Advanced Institute of Science and Technology, 291 Daehak-ro, Yuseong-gu, Daejeon 305-701, South Korea*
[2]*Department of Aerospace Engineering Sciences and Center for Aerospace Structures, University of Colorado, Campus Box 429, Boulder, CO 80309, USA*

SUMMARY

This paper presents a complete formulation for three-dimensional hydrodynamic analysis of floating flexible structures subjected to surface regular waves, as well as other excitation forces, by employing a direct tight coupling method. The continuum mechanics-based finite element method is employed to model floating structures with arbitrary geometries, which can account for the geometric nonlinearities and initial stress effects that result from the hydrostatic analysis, whereas the boundary element method is used for the fluid via total potential formulation. The simplicity and generality of the present formulation are revealed as compared with the conventional formulation. Numerical examples demonstrate the general capability of the formulation proposed. Copyright © 2013 John Wiley & Sons, Ltd.

Received 12 November 2012; Revised 20 June 2013; Accepted 1 August 2013

KEY WORDS: fluid-structure interaction; hydroelasticity; free surface gravity waves; direct coupling method; total velocity potential; Green's function; FEM; BEM

1. INTRODUCTION

For a long time, the dynamic analysis of floating structures that interact with surface regular waves has been typically based on the assumption of rigid body motions. Such analysis methods have been well developed after the inspiring works by John [1, 2]. The hydrodynamic rigid body motion analysis has been deemed adequate for the design of floating structures where rigid body motions are dominant. However, as the size of floating structures is getting larger to the extent that the flexible motions of floating structures account for a substantial portion of the hydrodynamic responses, the assumption of rigid body motions is no longer valid for the hydrodynamic analysis of floating structures.

With the increasing importance of hydroelasticity in water wave-structure interaction problems, hydroelastic analysis has attracted considerable interest. Most research efforts have focused on the analysis of very large floating structures (VLFSs) such as floating airports, pontoon-type offshore structures and bridges, and ice floes (see, e.g., Reference [3] for a survey of the hydroelastic analysis of VLFSs). In those studies, VLFSs have mostly been modeled by relatively simple beam or plate structures.

The conventional method for the hydroelastic analysis of floating structures (see, e.g., Reference [4]) uses the following steps, which is similar to the conventional hydrodynamic rigid body motion analysis method. First, the dynamic modes of a structure (usually dry modes or simple

*Correspondence to: Phill-Seung Lee, Division of Ocean Systems Engineering, Korea Advanced Institute of Science and Technology, 291 Daehak-ro, Yuseong-gu, Daejeon 305-701, South Korea.
†E-mail: phillseung@kaist.edu

mathematical modes) are calculated to construct the generalized coordinates. Second, the diffraction and radiation velocity potentials are calculated by solving the fluid equation, which is based on the potential flow theory. Third, the corresponding generalized coefficient matrices and forces (added mass, radiated wave damping, and wave excitation forces) are evaluated from the computed diffraction and radiation potentials. Finally, after computing the structural and hydrostatic stiffness that corresponds to the generalized coordinates, the generalized equations of motion for the floating structure are constructed and solved. The resulting analysis capability is limited to the linear hydroelastic analysis of floating structures. This method has been extended to 3D hydroelastic analysis by Wu [5] and Price and Wu [6].

Recently, several investigators (see, e.g., References [7–9]) have developed a direct coupling method in which the structural and fluid equations are directly coupled with each other, and the coupled equations are solved simultaneously. In contrast to the conventional method, this method does not require the effort of calculating the wave-structure interaction coefficients one by one. Therefore, there is no need to follow the conventional separated potential formulation [4, 10] where the problem is decomposed into diffraction and radiation problems [9]. In addition, the direct coupling method has an advantage in that it can be directly extended to the nonlinear analysis of floating structures. However, applications of the direct coupling method have focused on relatively simple floating beam or plate structures.

An important consideration for the general formulation of the 3D hydroelastic problem is the explicit inclusion of hydrostatic stiffness. The hydrostatic stiffness is related to the sum of the hydrostatic pressure and initial stress effects. Therefore, an explicit expression of load stiffness that is related to the hydrostatic pressure is needed, and the hydrostatic analysis should be preperformed before the hydrodynamic analysis. Huang and Riggs [11] gave attention to this fact and first proposed a complete hydrostatic stiffness coefficients that correspond to the structural modes.

Moreover, until now, most of the studies on the hydroelastic analysis of floating structures have focused on incident waves as the primary sources of external loads. However, not only wave excitation forces but also other various kinds of forces, such as engine excitation forces, mooring forces, and loading-induced and unloading-induced forces, have great impact on the behavior of floating structures. Thus, for a more general formulation for the 3D hydroelastic analysis of floating structures, the modeling of such forces should be additionally considered.

The objective of this paper is to present a complete formulation for the 3D hydroelastic analysis of floating structures. The present formulation is a generalization of the direct coupling method in steady state 3D hydroelastic problems, by employing the finite element and boundary element methods for floating structures and fluids, respectively. Representative features of the formulation include the following:

- Considering the geometrical nonlinearity of floating structures, the updated Lagrangian formulation of floating structures is derived and is consistently extended to the hydrostatic and steady state hydrodynamic analyses of floating structures.
- Total velocity potential formulation is employed for fluids, and an appropriate 3D boundary integral equation is newly derived.
- In the coupled equation, a complete hydrostatic stiffness is included, and all the interaction coefficients are put into one term. However, the term can be clearly decomposed by a condensation procedure.
- The modal analysis for structural dry modes is suggested in order to reduce the size of the resulting discrete coupled equation. Thus, the present formulation can secure computational efficiency.
- Harmonic surface forces are additionally formulated for the radiation problems of floating structures.

2. FORMULATION OF THE FLOATING STRUCTURE

We consider the interaction problem between floating structures and incident waves, as shown in Figure 1. The basic assumptions are that the structure has a homogeneous, isotropic, and linear

DOI: 10.1002/nme

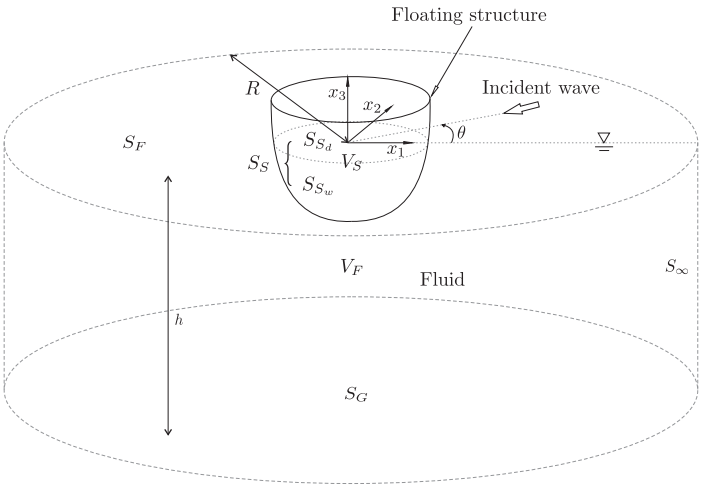

Figure 1. Problem description for a floating structure interacting with an incident wave.

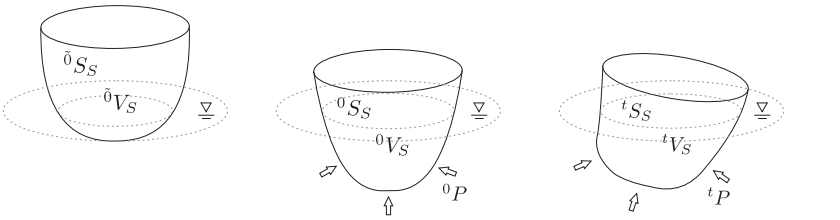

Figure 2. Three states of the problem: initial state, hydrostatic equilibrium state, and hydrodynamic equilibrium state.

elastic material and the fluid flow is incompressible, inviscid, and irrotational. The incident regular wave comes continuously from the positive x_1 axis with an angle θ, and the amplitude of it is small enough to use the linear wave theory. Also, the motion of the floating structure is assumed to be small. All the waves are gravity waves, and we ignore the surface tension effect. In addition, for simplicity, we set the atmospheric pressure as zero.

The volume occupied by the structure is V_S and by the fluid is V_F. The surface of structure S_S consists of wet and dry surfaces, which are denoted by S_{S_w} and S_{S_d}, respectively. The fluid is bounded by the wet surface of the structure S_{S_w}, the free surface S_F, the surface S_∞, which is a circular cylinder with a sufficiently large radius R, and the flat bottom surface S_G. The water depth h is measured from the flat bottom to the free surface of the calm water, and a fixed Cartesian coordinate system (x_1, x_2, x_3) on the free surface of the calm water is introduced.

For clear and compact notation, we introduce subscripts i and j, which vary from 1 to 3, to express the components of vector (or tensor) and adopt the Einstein summation convention.

To clarify the state of the problem, we classify it as three states, namely, the initial state, hydrostatic equilibrium state, and hydrodynamic equilibrium state as shown in Figure 2. The initial state is a virtual configuration obtained by an assumption of the static equilibrium state. We define these states as left superscripts $\tilde{0}$, 0, and t, respectively. The material point vectors for each state refer to $^{\tilde{0}}x_i$, $^{0}x_i$, and $^{t}x_i$, respectively. The displacement vectors are then defined by

$$\overset{0}{\tilde{0}}u_i = {}^{0}x_i - {}^{\tilde{0}}x_i, \quad \overset{t}{\tilde{0}}u_i = {}^{t}x_i - {}^{\tilde{0}}x_i, \quad \overset{t}{0}u_i = {}^{t}x_i - {}^{0}x_i. \tag{1}$$

The total pressure fields in the fluid are

$$^{0}P = -\rho_w g x_3, \quad {}^{t}P = -\rho_w g x_3 + {}^{t}P_D, \tag{2}$$

DOI: 10.1002/nme

where ρ_w is the density of the fluid (in this study, the fluid is water), g is the acceleration of gravity, and ${}^{t}P_D$ means the hydrodynamic pressure.

2.1. Updated Lagrangian formulation

The procedure for the structural formulation consists of two steps, that is, the hydrostatic analysis focused on the static equilibrium state and the hydrodynamic analysis treating the dynamic equilibrium state. Although the main problem in this study is the hydrodynamic analysis, the hydrostatic analysis is important in the present structural formulation. The main reason is that, as mentioned in the Section 1, the Cauchy stress tensor in the static equilibrium state influences the accurate evaluation of the hydrostatic stiffness in the dynamic equilibrium state.

To obtain the formulations corresponding to each problem, we adopt the updated Lagrangian formulation [12]. The equilibrium equations of the floating structure at time $\tau + \Delta\tau$ are

$$\begin{aligned} \frac{\partial {}^{\tau+\Delta\tau}\sigma_{ij}}{\partial {}^{\tau+\Delta\tau}x_j} - {}^{\tau+\Delta\tau}\rho_s g\delta_{i3} - {}^{\tau+\Delta\tau}\rho_s {}^{\tau+\Delta\tau}\ddot{x}_i = 0 \quad & \text{in } {}^{\tau+\Delta\tau}V_S, \\ {}^{\tau+\Delta\tau}\sigma_{ij}\,{}^{\tau+\Delta\tau}n_j = -{}^{\tau+\Delta\tau}P\,{}^{\tau+\Delta\tau}n_i \quad & \text{on } {}^{\tau+\Delta\tau}S_{S_w} \\ {}^{\tau+\Delta\tau}\sigma_{ij}\,{}^{\tau+\Delta\tau}n_j = 0 \quad & \text{on } {}^{\tau+\Delta\tau}S_{S_d}, \end{aligned} \tag{3}$$

where σ_{ij} is the Cauchy stress tensor, ρ_s is the density of the structure, n_i is the unit normal vector outward from the structure to the fluid, and δ_{ij} is the Kronecker delta. In the aforementioned equation, we assume that the body force per unit mass applied to the structure is the acceleration of gravity g in the negative x_3 direction. Also, we use the overdot to represent the material time derivative.

Then, the principle of virtual displacements at time $\tau + \Delta\tau$ can be stated as

$$\int_{{}^{\tau+\Delta\tau}V_S} {}^{\tau+\Delta\tau}\sigma_{ij}\,{}^{\tau+\Delta\tau}\bar{e}_{ij}\,\mathrm{d}V \tag{4a}$$

$$= -\int_{{}^{\tau+\Delta\tau}V_S} {}^{\tau+\Delta\tau}\rho_s g\bar{u}_3\,\mathrm{d}V \tag{4b}$$

$$+ \int_{{}^{\tau+\Delta\tau}S_{S_w}} \rho_w g\,{}^{\tau+\Delta\tau}x_3\,{}^{\tau+\Delta\tau}n_i\bar{u}_i\,\mathrm{d}S \tag{4c}$$

$$- \int_{{}^{\tau+\Delta\tau}S_{S_w}} {}^{\tau+\Delta\tau}P_D\,{}^{\tau+\Delta\tau}n_i\bar{u}_i\,\mathrm{d}S \tag{4d}$$

$$- \int_{{}^{\tau+\Delta\tau}V_S} {}^{\tau+\Delta\tau}\rho_s\,{}^{\tau+\Delta\tau}_{\tilde{0}}\ddot{u}_i\bar{u}_i\,\mathrm{d}V, \tag{4e}$$

where ${}^{\tau+\Delta\tau}_{\tilde{0}}u_i$ is the displacement from the configuration at time $\tilde{0}$ to the configuration at time $\tau + \Delta\tau$, $\bar{u}_i$ is the virtual displacement vector imposed on the configuration at time $\tau + \Delta\tau$, and ${}_{\tau+\Delta\tau}\bar{e}_{ij}$ is the virtual strain tensor that corresponds to the virtual displacements $\bar{u}_i$, which is

$${}_{\tau+\Delta\tau}\bar{e}_{ij} = \frac{1}{2}\left(\frac{\partial \bar{u}_i}{\partial {}^{\tau+\Delta\tau}x_j} + \frac{\partial \bar{u}_j}{\partial {}^{\tau+\Delta\tau}x_i}\right). \tag{5}$$

Equation (4a) can be transformed and linearized as (see, e.g., Reference [12])

$$\begin{aligned} \int_{{}^{\tau+\Delta\tau}V_S} {}^{\tau+\Delta\tau}\sigma_{ij}\,{}^{\tau+\Delta\tau}\bar{e}_{ij}\,\mathrm{d}V \approx \int_{{}^{\tau}V_S} C_{ijkl}\,{}^{\tau+\Delta\tau}_{\tau}e_{kl}\,{}_{\tau}\bar{e}_{ij}\,\mathrm{d}V + \int_{{}^{\tau}V_S} {}^{\tau}\sigma_{ij}\,{}^{\tau+\Delta\tau}_{\tau}\bar{\eta}_{ij}\,\mathrm{d}V \\ + \int_{{}^{\tau}V_S} {}^{\tau}\sigma_{ij}\,{}_{\tau}\bar{e}_{ij}\,\mathrm{d}V, \end{aligned} \tag{6}$$

DOI: 10.1002/nme

where

$$
\begin{aligned}
{}^{\tau+\Delta\tau}_{\tau}e_{ij} &= \frac{1}{2}\left(\frac{\partial^{\tau+\Delta\tau}_{\tau}u_i}{\partial^{\tau}x_j}+\frac{\partial^{\tau+\Delta\tau}_{\tau}u_j}{\partial^{\tau}x_i}\right),\\
{}_{\tau}\bar{e}_{ij} &= \frac{1}{2}\left(\frac{\partial\bar{u}_i}{\partial^{\tau}x_j}+\frac{\partial\bar{u}_j}{\partial^{\tau}x_i}\right), \quad {}^{\tau+\Delta\tau}_{\tau}\bar{\eta}_{ij} = \frac{1}{2}\left(\frac{\partial\bar{u}_k}{\partial^{\tau}x_i}\frac{\partial^{\tau+\Delta\tau}_{\tau}u_k}{\partial^{\tau}x_j}+\frac{\partial^{\tau+\Delta\tau}_{\tau}u_k}{\partial^{\tau}x_i}\frac{\partial\bar{u}_k}{\partial^{\tau}x_j}\right).
\end{aligned}
\tag{7}
$$

In the aforementioned equations, ${}^{\tau+\Delta\tau}_{\tau}u_i$ is the displacement from the configuration at time τ to the configuration at time $\tau+\Delta\tau$, and C_{ijkl} is the stress-strain relation tensor.

We can also linearize the term (4c) as

$$
\begin{aligned}
\int_{{}^{\tau+\Delta\tau}S_{S_w}}\rho_w g\,{}^{\tau+\Delta\tau}x_3\,{}^{\tau+\Delta\tau}n_i\bar{u}_i\,\mathrm{d}S \approx &\int_{{}^{\tau}S_{S_w}}\rho_w g\,{}^{\tau}x_3\,{}^{\tau}n_i\bar{u}_i\,\mathrm{d}S\\
&+\int_{{}^{\tau}S_{S_w}}\rho_w g\,{}^{\tau+\Delta\tau}_{\tau}u_3\,{}^{\tau}n_i\bar{u}_i\,\mathrm{d}S\\
&+\int_{{}^{\tau}S_{S_w}}\rho_w g\,{}^{\tau}x_3\,{}^{\tau}n_j\,{}^{\tau}_{\tau+\Delta\tau}\mathcal{F}_{ij}\bar{u}_i\,\mathrm{d}S,
\end{aligned}
\tag{8}
$$

where ${}^{\tau}_{\tau+\Delta\tau}\mathcal{F}_{ij}$ is defined as

$${}^{\tau}_{\tau+\Delta\tau}\mathcal{F}_{ij} = \delta_{ij}\frac{\partial^{\tau+\Delta\tau}_{\tau}u_k}{\partial^{\tau}x_k}-\frac{\partial^{\tau+\Delta\tau}_{\tau}u_j}{\partial^{\tau}x_i}. \tag{9}$$

Another linearized form for this term can also be found in Reference [13], which is actually the same as the expression on the right-hand side of Equation (8).

Similarly, the term (4d) can be linearized by recalling that the hydrodynamic pressure ${}^{\tau+\Delta\tau}P_D$ is an unknown variable:

$$\int_{{}^{\tau+\Delta\tau}S_{S_w}}{}^{\tau+\Delta\tau}P_D\,{}^{\tau+\Delta\tau}n_i\bar{u}_i\,\mathrm{d}S = \int_{{}^{\tau}S_{S_w}}{}^{\tau+\Delta\tau}P_D\,{}^{\tau}n_i\bar{u}_i\,\mathrm{d}S. \tag{10}$$

Then, by substituting the terms (4a), (4c), and (4d) with (6), (8), and (10), respectively, and applying the relation ${}^{\tau+\Delta\tau}\rho_s\,\mathrm{d}^{\tau+\Delta\tau}V = {}^{\tau}\rho_s\,\mathrm{d}^{\tau}V$ to the terms (4b) and (4e), we obtain the following linearized form:

$$
\begin{aligned}
&\int_{{}^{\tau}V_S}{}^{\tau}\rho_s\,{}^{\tau+\Delta\tau}_{\bar{0}}\ddot{u}_i\bar{u}_i\,\mathrm{d}V+\int_{{}^{\tau}V_S}C_{ijkl}\,{}^{\tau+\Delta\tau}_{\tau}e_{kl}\,{}_{\tau}\bar{e}_{ij}\,\mathrm{d}V+\int_{{}^{\tau}V_S}{}^{\tau}\sigma_{ij}\,{}^{\tau+\Delta\tau}_{\tau}\bar{\eta}_{ij}\,\mathrm{d}V\\
&\quad-\int_{{}^{\tau}S_{S_w}}\rho_w g\,{}^{\tau+\Delta\tau}_{\tau}u_3\,{}^{\tau}n_i\bar{u}_i\,\mathrm{d}S-\int_{{}^{\tau}S_{S_w}}\rho_w g\,{}^{\tau}x_3\,{}^{\tau}n_j\,{}^{\tau}_{\tau+\Delta\tau}\mathcal{F}_{ij}\bar{u}_i\,\mathrm{d}S\\
&\quad+\int_{{}^{\tau}S_{S_w}}{}^{\tau+\Delta\tau}P_D\,{}^{\tau}n_i\bar{u}_i\,\mathrm{d}S=-\int_{{}^{\tau}V_S}{}^{\tau}\rho_s g\bar{u}_3\,\mathrm{d}V\\
&\quad+\int_{{}^{\tau}S_{S_w}}\rho_w g\,{}^{\tau}x_3\,{}^{\tau}n_i\bar{u}_i\,\mathrm{d}S-\int_{{}^{\tau}V_S}{}^{\tau}\sigma_{ij}\,{}_{\tau}\bar{e}_{ij}\,\mathrm{d}V.
\end{aligned}
\tag{11}
$$

Note that the problems considered in this section involve nonlinear effects mainly due to the change of the wet surface. Therefore, an iterative solution method should be employed with Equation (11) (see, e.g., Reference [12]).

2.2. *Hydrostatic analysis*

Under the initial configuration where the wet surface exists, we can find the solution of the hydrostatic problem by using Equation (11). In this case, the acceleration ${}^{0}_{\bar{0}}\ddot{u}_i$ and the hydrodynamic pressure ${}^{0}P_D$ are equal to zero. Then, Equation (11) becomes

DOI: 10.1002/nme

$$\int_{\tilde{0}V_S} C_{ijkl}\,{}^{0}_{\tilde{0}}e_{kl}\,{}_{\tilde{0}}\bar{e}_{ij}\,\mathrm{d}V + \int_{\tilde{0}V_S} {}^{\tilde{0}}\sigma_{ij}\,{}^{0}_{\tilde{0}}\bar{\eta}_{ij}\,\mathrm{d}V - \int_{\tilde{0}S_{S_w}} \rho_w g\,{}^{0}_{\tilde{0}}u_3\,{}^{\tilde{0}}n_i\bar{u}_i\,\mathrm{d}S$$
$$- \int_{\tilde{0}S_{S_w}} \rho_w g\,{}^{\tilde{0}}x_3\,{}^{\tilde{0}}n_j\,{}^{\tilde{0}}_{0}\mathcal{F}_{ij}\bar{u}_i\,\mathrm{d}S = -\int_{\tilde{0}V_S} {}^{\tilde{0}}\rho_s g\bar{u}_3\,\mathrm{d}V \qquad (12)$$
$$+ \int_{\tilde{0}S_{S_w}} \rho_w g\,{}^{\tilde{0}}x_3\,{}^{\tilde{0}}n_i\bar{u}_i\,\mathrm{d}S - \int_{\tilde{0}V_S} {}^{\tilde{0}}\sigma_{ij}\,{}_{\tilde{0}}\bar{e}_{ij}\,\mathrm{d}V.$$

It should be noted that we do not assume that the displacement ${}^{0}_{\tilde{0}}u_i$ and the difference between the wet surface of the initial state and the wet surface of the static equilibrium state are small. Thus, an iterative solution method needs to be applied to Equation (12).

2.3. Hydrodynamic analysis in the steady state

In this case, the nonlinear effects can be ignored because we assume that the motions of the floating structure are small, and the change of the wet surface is negligible. Thus, we can use Equation (11) without employing an iterative solution method.

The reference configuration for the hydrodynamic analysis is the static equilibrium state that is obtained by the previous hydrostatic analysis. The condition for the state can be written as

$$-\int_{0V_S} {}^{0}\rho_s g\bar{u}_3\,\mathrm{d}V + \int_{0S_{S_w}} \rho_w g\,{}^{0}x_3\,{}^{0}n_i\bar{u}_i\,\mathrm{d}S - \int_{0V_S} {}^{0}\sigma_{ij}\,{}_{0}\bar{e}_{ij}\,\mathrm{d}V = 0. \qquad (13)$$

Invoking harmonic response under the harmonic excitation of the hydrodynamic pressure, that is, ${}^{t}_{0}u_i = \mathrm{Re}\left\{u_i({}^{0}\mathbf{x})e^{j\omega t}\right\};\ j=\sqrt{-1}$, we then obtain the following steady state equation:

$$-\omega^2\int_{0V_S} {}^{0}\rho_s u_i\bar{u}_i\,\mathrm{d}V + \int_{0V_S} C_{ijkl}e_{kl}\,{}_{0}\bar{e}_{ij}\,\mathrm{d}V + \int_{0V_S} {}^{0}\sigma_{ij}\bar{\eta}_{ij}\,\mathrm{d}V$$
$$-\int_{0S_{S_w}} \rho_w g u_3\,{}^{0}n_i\bar{u}_i\,\mathrm{d}S - \int_{0S_{S_w}} \rho_w g\,{}^{0}x_3\,{}^{0}n_j\mathcal{F}_{ij}\bar{u}_i\,\mathrm{d}S + \int_{0S_{S_w}} P_D\,{}^{0}n_i\bar{u}_i\,\mathrm{d}S = 0, \qquad (14)$$

where

$${}^{t}_{0}e_{ij} = \mathrm{Re}\left\{e_{ij}\left({}^{0}\mathbf{x}\right)e^{j\omega t}\right\},\quad {}^{t}_{0}\bar{\eta}_{ij} = \mathrm{Re}\left\{\bar{\eta}_{ij}\left({}^{0}\mathbf{x}\right)e^{j\omega t}\right\},$$
$${}^{0}_{t}\mathcal{F}_{ij} = \mathrm{Re}\left\{\mathcal{F}_{ij}\left({}^{0}\mathbf{x}\right)e^{j\omega t}\right\},\quad {}^{t}P_D = \mathrm{Re}\left\{P_D\left({}^{0}\mathbf{x}\right)e^{j\omega t}\right\}. \qquad (15)$$

3. FORMULATION OF THE FLUID

In the steady state, the velocity potential ${}^{t}\phi$ is governed by

$${}^{t}\phi = \mathrm{Re}\left\{\phi(\mathbf{x})e^{j\omega t}\right\}, \qquad (16a)$$
$$\nabla^2\phi = 0 \qquad \text{in } {}^{0}V_F, \qquad (16b)$$
$$\frac{\partial\phi}{\partial x_3} = \frac{\omega^2}{g}\phi \qquad \text{for } x_3 = 0 \text{ on } S_F, \qquad (16c)$$
$$\frac{\partial\phi}{\partial x_3} = 0 \qquad \text{on } S_G\ (x_3 = -h), \qquad (16d)$$
$$\sqrt{R}\left(\frac{\partial}{\partial R} + jk\right)(\phi - \phi^I) = 0 \qquad \text{on } S_\infty\ (R\to\infty), \qquad (16e)$$
$$\frac{\partial\phi}{\partial n} = j\omega u_i n_i \qquad \text{on } {}^{0}S_{S_w}, \qquad (16f)$$

where ∇^2 is the Laplace operator, k is the wave number, and ϕ^I is the velocity potential for the incident wave. The condition (16c) is the combined free surface boundary condition in which the

DOI: 10.1002/nme

kinematic and dynamic free surface boundary conditions are linearized at $x_3 = 0$ [14, 15], and the condition (16e) is the Sommerfeld radiation condition, which means that the diffracted and radiated waves should be outgoing waves [14]. The condition (16f) means that the velocities of structure and fluid, which are normal to the wet boundary surface, should be the same as each other on the wet surface. Note that the conditions (16b) and (16f) are approximated at the configuration of the static equilibrium state.

The incident velocity potential ϕ^I is defined by (see, e.g., References [14, 15])

$$\phi^I = j\frac{ga}{\omega}\frac{\cosh k(x_3+h)}{\cosh kh}e^{jk(x_1\cos\theta+x_2\sin\theta)}, \tag{17}$$

for the finite depth case, and

$$\phi^I = j\frac{ga}{\omega}e^{kx_3}e^{jk(x_1\cos\theta+x_2\sin\theta)}, \tag{18}$$

for the infinite depth case where a is the amplitude of the incident wave.

The angular frequency ω and the wave number k are related by the following dispersion relation:

$$k\sinh kh - \frac{\omega^2}{g}\cosh kh = 0 \quad \text{for the finite depth case and}$$
$$k - \frac{\omega^2}{g} = 0 \quad \text{for the infinite depth case.} \tag{19}$$

3.1. Free surface Green's function

The free surface Green's function that we use is a velocity potential generated by a source potential with strength -4π, which is located at position ξ_i and pulsated with the angular frequency ω. It satisfies the following conditions:

$$^{\mathrm{t}}G = \mathrm{Re}\left\{G(\mathbf{x};\boldsymbol{\xi})e^{j\omega t}\right\}, \tag{20a}$$
$$\nabla^2 G = -4\pi\delta(x_1-\xi_1)\delta(x_2-\xi_2)\delta(x_3-\xi_3) \quad \text{for } -h < x_3 < 0, \tag{20b}$$
$$\frac{\partial G}{\partial x_3} = \frac{\omega^2}{g}G \quad \text{for } x_3 = 0 \text{ and } x_i \neq \xi_i, \tag{20c}$$
$$\frac{\partial G}{\partial x_3} = 0 \quad \text{for } x_3 = -h \text{ and } x_i \neq \xi_i, \tag{20d}$$
$$\sqrt{r}\left(\frac{\partial}{\partial r} + jk\right)G = 0 \quad \text{as } r \to \infty, \tag{20e}$$

where δ is the Dirac's delta function and $r = \sqrt{(x_1-\xi_1)^2+(x_2-\xi_2)^2}$.

The detailed procedure to obtain the Green's function in finite and infinite depth cases is well explained by John [2] and Wehausen and Laitone [14]. The results are

$$G(\mathbf{x};\boldsymbol{\xi}) = \frac{1}{\sqrt{r^2+(x_3-\xi_3)^2}} + \frac{1}{\sqrt{r^2+(2h+x_3+\xi_3)^2}} + 2\int_{\mathcal{C}} \frac{\left(z+\frac{\omega^2}{g}\right)\cosh z(x_3+h)\cosh z(\xi_3+h)}{z\sinh zh - \frac{\omega^2}{g}\cosh zh} e^{-zh}J_0(zr)\,\mathrm{d}z, \tag{21}$$

for the finite depth case, and

$$G(\mathbf{x};\boldsymbol{\xi}) = \frac{1}{\sqrt{r^2+(x_3-\xi_3)^2}} + \int_{\mathcal{C}} \frac{z+\frac{\omega^2}{g}}{z-\frac{\omega^2}{g}} e^{-z|x_3+\xi_3|}J_0(zr)\,\mathrm{d}z, \tag{22}$$

for the infinite depth case, where J_0 is the Bessel function of the first kind of order 0. The path $\mathcal{C}$ of integral in Equations (21) and (22) is indented above the pole k_0 so that it runs a half circle

DOI: 10.1002/nme

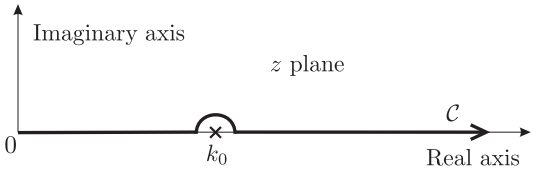

Figure 3. Integral path in the Green's function.

with a very small radius in the complex plane z as shown in Figure 3. The pole k_0 is the positive real root of the equations $z \tanh zh = \omega^2/g$ for the finite depth case and $z = \omega^2/g$ for the infinite depth case.

For the singular or near-singular characteristics of the Green's function for the region, $-h < x_3 \leqq 0$ and $-h < \xi_3 \leqq 0$, we can decompose the Green's function into singular, nearly singulars, and regular parts as (References [2, 16])

$$G(\mathbf{x};\boldsymbol{\xi}) = \frac{1}{\sqrt{r^2+(x_3-\xi_3)^2}} + \frac{1}{\sqrt{r^2+(x_3+\xi_3)^2}} - 2\frac{\omega^2}{g} e^{\frac{\omega^2}{g}(x_3+\xi_3)} \ln\left\{\sqrt{r^2+(x_3+\xi_3)^2} - (x_3+\xi_3)\right\} + \tilde{G} \text{ (regular terms).} \tag{23}$$

3.2. Boundary integral equation

By using the Green's theorem and the Green's function, we can derive a useful form from the expressions (16b)$\sim$ (16e) and (20b)$\sim$ (20e). The starting point is the Green's second identity for ϕ and G:

$$\int_{{}^0V_F} \left\{\nabla^2 G(\mathbf{x};\boldsymbol{\xi})\phi(\mathbf{x}) - G(\mathbf{x};\boldsymbol{\xi})\nabla^2\phi(\mathbf{x})\right\} \mathrm{d}V_x = \int_{{}^0S_C} \left\{\frac{\partial G(\mathbf{x};\boldsymbol{\xi})}{\partial n'(\mathbf{x})}\phi(\mathbf{x}) - G(\mathbf{x};\boldsymbol{\xi})\frac{\partial\phi(\mathbf{x})}{\partial n'(\mathbf{x})}\right\} \mathrm{d}S_x, \tag{24}$$

where ${}^0S_C$ is the closed boundary surface that envelops the fluid domain ${}^0V_F$, and n_i' is the unit normal vector outward from the fluid region, that is, $n_i = -n_i'$ at the wet surface ${}^0S_{S_w}$. The subscript x in the aforementioned expression means that the integral is conducted with respect to the variable x_i.

By invoking the commutative property of the Green's function, that is, $G(\mathbf{x};\boldsymbol{\xi}) = G(\boldsymbol{\xi};\mathbf{x})$, the conditions (20b)$\sim$ (20e) are also valid if we reconstitute them with respect to ξ_i. Thus, for the case where the spatial position x_i is on the wet surface ${}^0S_{S_w}$, we can rewrite the integrals in Equation (24) with respect to ξ_i. We then have, after applying the boundary conditions (16c) $\sim$ (16e) of the velocity potential ϕ and the conditions (20c)$\sim$ (20e) of the Green's function G for each surface,

$$-\alpha\phi(\mathbf{x}) = \text{⨍}_{{}^0S_{S_w}} \left\{\frac{\partial G(\mathbf{x};\boldsymbol{\xi})}{\partial n'(\boldsymbol{\xi})}\phi(\boldsymbol{\xi}) - G(\mathbf{x};\boldsymbol{\xi})\frac{\partial\phi(\boldsymbol{\xi})}{\partial n'(\boldsymbol{\xi})}\right\} \mathrm{d}S_\xi + \int_{S_\infty} \left\{\frac{\partial G(\mathbf{x};\boldsymbol{\xi})}{\partial n'(\boldsymbol{\xi})}\phi^I(\boldsymbol{\xi}) - G(\mathbf{x};\boldsymbol{\xi})\frac{\partial\phi^I(\boldsymbol{\xi})}{\partial n'(\boldsymbol{\xi})}\right\} \mathrm{d}S_\xi \quad \text{for } \mathbf{x} \text{ on } {}^0S_{S_w}, \tag{25}$$

where α is the solid angle of the fluid measured from x_i; when x_i is at the intersecting line of the wet surface and the free surface, it is two times the solid angle (see, e.g., Reference [17]). The middle-dashed integral sign refers to the Cauchy principal value, and the subscript ξ means that the integral is conducted with respect to the variable ξ_i.

We can also apply the same procedure for the incident velocity potential ϕ^I and the Green's function G in the region that contains ${}^0V_F$ and the displaced volume ${}^0V_d$. After applying the combined free surface boundary condition and the bottom boundary condition of the Green's function

DOI: 10.1002/nme

G (Equations (20c) and (20d)) and the incident potential ϕ^I, the Green's second identity for ϕ^I and G becomes

$$-4\pi\phi^I(\mathbf{x}) = \int_{S_\infty} \left\{ \frac{\partial G(\mathbf{x};\boldsymbol{\xi})}{\partial n'(\boldsymbol{\xi})}\phi^I(\boldsymbol{\xi}) - G(\mathbf{x};\boldsymbol{\xi})\frac{\partial \phi^I(\boldsymbol{\xi})}{\partial n'(\boldsymbol{\xi})} \right\} \mathrm{d}S_\xi \quad \text{for } \mathbf{x} \text{ on } {}^0S_{S_w}. \tag{26}$$

If we subtract Equation (26) from Equation (25) and apply the relation $n_i' = -n_i$, then we finally obtain

$$\alpha\phi(\mathbf{x}) - \fint_{{}^0S_{S_w}} \frac{\partial G(\mathbf{x};\boldsymbol{\xi})}{\partial n(\boldsymbol{\xi})}\phi(\boldsymbol{\xi})\,\mathrm{d}S_\xi = -\fint_{{}^0S_{S_w}} G(\mathbf{x};\boldsymbol{\xi})\frac{\partial \phi(\boldsymbol{\xi})}{\partial n(\boldsymbol{\xi})}\,\mathrm{d}S_\xi + 4\pi\phi^I(\mathbf{x}) \quad \text{for } \mathbf{x} \text{ on } {}^0S_{S_w}. \tag{27}$$

It should be noted that according to the Fredholm integral equation theory, Equation (27) has either no solution or nonunique solutions at what are termed irregular frequencies, where the solutions of the associated homogeneous integral equation (the equation where the right-hand side of Equation (27) is zero) are nontrivial. In the corresponding discrete equation, the coefficient matrix becomes ill-conditioned near the irregular frequencies. A successful method that can be used to remove the irregular frequency effects was developed by Ohmatsu [18] and Kleinman [19], relying on extended boundary integral equations. Details of this method can be found in Reference [20]. However, for simplicity, we do not apply a method to remove the irregular frequency effects to Equation (27).

For subsequent boundary element approximations, we weigh a test function $\bar{\phi}$ to Equation (27) and integrate over the surface ${}^0S_{S_W}$:

$$\alpha\int_{{}^0S_{S_w}} \phi\bar{\phi}\,\mathrm{d}S - \int_{{}^0S_{S_w}}\fint_{{}^0S_{S_w}} \left(\frac{\partial G}{\partial n_\xi}\phi - G\frac{\partial \phi}{\partial n_\xi}\right)\mathrm{d}S_\xi\bar{\phi}\,\mathrm{d}S_x = 4\pi\int_{{}^0S_{S_w}} \phi^I\bar{\phi}\,\mathrm{d}S. \tag{28}$$

3.3. Coupled formulation for the steady state

Now, we obtain coupled equations from the formulations of the floating structure (14) and the fluid (28) by the Bernoulli equation and the interface Equation (16f). The Bernoulli equation used in this study is also linearized at the static equilibrium configuration. Thus, the hydrodynamic pressure P_D can be expressed as

$$P_D = -j\omega\rho_w\phi. \tag{29}$$

By substituting the aforementioned equation into Equation (14) and the condition (16f) into Equation (28), we finally obtain the coupled structural and fluid equations:

$$-\omega^2\int_{{}^0V_S} {}^0\rho_s u_i\bar{u}_i\,\mathrm{d}V + \int_{{}^0V_S} C_{ijkl}e_{kl}\,{}^0\bar{e}_{ij}\,\mathrm{d}V + \int_{{}^0V_S} {}^0\sigma_{ij}\bar{\eta}_{ij}\,\mathrm{d}V - \int_{{}^0S_{S_w}} \rho_w g u_3\,{}^0n_i\bar{u}_i\,\mathrm{d}S - \int_{{}^0S_{S_w}} \rho_w g\,{}^0x_3\,{}^0n_j\mathcal{F}_{ij}\bar{u}_i\,\mathrm{d}S - j\omega\int_{{}^0S_{S_w}} \rho_w\phi\,{}^0n_i\bar{u}_i\,\mathrm{d}S = 0, \tag{30}$$

and

$$\alpha\int_{{}^0S_{S_w}} \phi\bar{\phi}\,\mathrm{d}S - \int_{{}^0S_{S_w}}\fint_{{}^0S_{S_w}} \left(\frac{\partial G}{\partial n_\xi}\phi - j\omega G u_i n_i\right)\mathrm{d}S_\xi\bar{\phi}\,\mathrm{d}S_x = 4\pi\int_{{}^0S_{S_w}} \phi^I\bar{\phi}\,\mathrm{d}S. \tag{31}$$

DOI: 10.1002/nme

4. FINITE AND BOUNDARY ELEMENT PROCEDURES

In this section, we derive matrix formulations for the steady state hydrodynamic problems by spatial discretization. Term-by-term finite element discretization of the linearized structural Equation (30) yields

$$\omega^2 \int_{{}^0V_S} {}^0\rho_s u_i \bar{u}_i \, \mathrm{d}V = \hat{\bar{\mathbf{u}}}^{\mathrm{T}} \omega^2 \mathbf{S}_M \hat{\mathbf{u}}, \tag{32a}$$

$$\int_{{}^0V_S} C_{ijkl} e_{kl} \, {}^0\bar{e}_{ij} \, \mathrm{d}V = \hat{\bar{\mathbf{u}}}^{\mathrm{T}} \mathbf{S}_K \hat{\mathbf{u}}, \tag{32b}$$

$$\int_{{}^0V_S} {}^0\sigma_{ij} \bar{\eta}_{ij} \, \mathrm{d}V = \hat{\bar{\mathbf{u}}}^{\mathrm{T}} \mathbf{S}_{KN} \hat{\mathbf{u}}, \tag{32c}$$

$$\int_{{}^0S_{S_w}} \rho_w g u_3 \, {}^0n_i \bar{u}_i \, \mathrm{d}S = \hat{\bar{\mathbf{u}}}^{\mathrm{T}} \mathbf{S}_{HD} \hat{\mathbf{u}}, \tag{32d}$$

$$\int_{{}^0S_{S_w}} \rho_w g \, {}^0x_3 \, {}^0n_j \mathcal{F}_{ij} \bar{u}_i \, \mathrm{d}S = \hat{\bar{\mathbf{u}}}^{\mathrm{T}} \mathbf{S}_{HN} \hat{\mathbf{u}}, \tag{32e}$$

$$j\omega \int_{{}^0S_{S_w}} \rho_w \phi \, {}^0n_i \bar{u}_i \, \mathrm{d}S = \hat{\bar{\mathbf{u}}}^{\mathrm{T}} j\omega \mathbf{S}_D \hat{\boldsymbol{\phi}}. \tag{32f}$$

Similarly, term-by-term boundary element discretization of the fluid Equation (31) yields

$$\alpha \int_{{}^0S_{S_w}} \phi \bar{\phi} \, \mathrm{d}S = \hat{\bar{\boldsymbol{\phi}}}^{\mathrm{T}} \alpha \mathbf{F}_M \hat{\boldsymbol{\phi}}, \tag{33a}$$

$$\int_{{}^0S_{S_w}} \oint_{{}^0S_{S_w}} \frac{\partial G}{\partial n_\xi} \phi \, \mathrm{d}S_\xi \bar{\phi} \, \mathrm{d}S_x = \hat{\bar{\boldsymbol{\phi}}}^{\mathrm{T}} \mathbf{F}_{Gn} \hat{\boldsymbol{\phi}}, \tag{33b}$$

$$j\omega \int_{{}^0S_{S_w}} \oint_{{}^0S_{S_w}} G u_i n_i \, \mathrm{d}S_\xi \bar{\phi} \, \mathrm{d}S_x = \hat{\bar{\boldsymbol{\phi}}}^{\mathrm{T}} j\omega \mathbf{F}_G \hat{\mathbf{u}}, \tag{33c}$$

$$4\pi \int_{{}^0S_{S_w}} \phi^I \bar{\phi} \, \mathrm{d}S = \hat{\bar{\boldsymbol{\phi}}}^{\mathrm{T}} 4\pi \mathbf{R}_I. \tag{33d}$$

In the aforementioned expressions, $\hat{\mathbf{u}}$ and $\hat{\boldsymbol{\phi}}$ mean nodal displacement and velocity potential vectors, respectively.

Hence, the discrete coupled equation for the steady state 3D hydroelastic problems can be written as

$$\begin{bmatrix} -\omega^2 \mathbf{S}_M + \mathbf{S}_K + \mathbf{S}_{KN} - \mathbf{S}_{HD} - \mathbf{S}_{HN} & -j\omega \mathbf{S}_D \\ j\omega \mathbf{F}_G & \alpha \mathbf{F}_M - \mathbf{F}_{Gn} \end{bmatrix} \begin{bmatrix} \hat{\mathbf{u}} \\ \hat{\boldsymbol{\phi}} \end{bmatrix} = \begin{bmatrix} 0 \\ 4\pi \mathbf{R}_I \end{bmatrix}. \tag{34}$$

Note that the matrix '$\mathbf{S}_{KN} - \mathbf{S}_{HD} - \mathbf{S}_{HN}$' is the complete hydrostatic stiffness for the floating structure.

4.1. Condensed structural equation

Eatock Taylor [9] showed that by condensing out the fluid variable in his wave-plate structure interaction formula, all the interaction terms can be clearly decomposed. Similarly, our discrete coupled equation can be transformed to a condensed structural equation where the added mass, radiated wave damping, and wave excitation forces are clearly extracted.

In the fluid part of Equation (34), $\hat{\boldsymbol{\phi}}$ can be expressed as

$$\hat{\boldsymbol{\phi}} = (\alpha \mathbf{F}_M - \mathbf{F}_{Gn})^{-1} (4\pi \mathbf{R}_I - j\omega \mathbf{F}_G \hat{\mathbf{u}}). \tag{35}$$

If we insert Equation (35) into the structural part of Equation (34), we obtain the following condensed structural equation for the steady state 3D hydroelastic problems:

$$\left[-\omega^2 (\mathbf{S}_M + \mathbf{S}_{MA}) + j\omega \mathbf{S}_{CW} + \mathbf{S}_K + \mathbf{S}_{KN} - \mathbf{S}_{HD} - \mathbf{S}_{HN}\right] \hat{\mathbf{u}} = \mathbf{R}_W, \tag{36}$$

DOI: 10.1002/nme

where

$$\begin{aligned}
\mathbf{S}_{MA} &= \mathrm{Re}\left\{\mathbf{S}_D\left(\alpha\mathbf{F}_M - \mathbf{F}_{Gn}\right)^{-1}\mathbf{F}_G\right\} && \text{: added mass matrix,}\\
\mathbf{S}_{CW} &= -\omega \times \mathrm{Im}\left\{\mathbf{S}_D\left(\alpha\mathbf{F}_M - \mathbf{F}_{Gn}\right)^{-1}\mathbf{F}_G\right\} && \text{: radiated wave damping matrix,}\\
\mathbf{R}_W &= j\omega\mathbf{S}_D\left(\alpha\mathbf{F}_M - \mathbf{F}_{Gn}\right)^{-1} 4\pi\mathbf{R}_I && \text{: wave excitation forces matrix.}
\end{aligned} \tag{37}$$

4.2. Remarks on the numerical evaluations

There are some important considerations related to the calculations of Equation (34) and the terms (33b) and (33c). First, the integral form of Green's function and its derivatives are hard to efficiently evaluate (Equations (21) and (22)). Because the number of calculations that contain them is proportional to the square of the number of the fluid boundary elements, a time-efficient form is necessary. Newman [16, 21] developed an efficient numerical algorithm for evaluating the Green's function and its derivatives using analytical series expansions and polynomials approximation by dividing the relevant domain.

The second consideration is related to the singular and nearly singular integrals that we encounter when constructing the matrices (33b) and (33c). The outer integrals of the terms (33b) and (33c) can be carried out by the Gauss–Legendre quadrature, but the inner integral should be computed differently because of the singular and nearly singular components of the Green's function.

Let us see the inner integral in detail. Because the singular or nearly singular components of the Green's function can be divided as shown in Equation (23), the inner integrals of the terms (33c) and (33b) can be decomposed as

$$\begin{aligned}
&\int_{0S_{Sw}^{(e)}} G\mathbf{n}^{\mathrm{T}}\mathbf{H}_S^{(e)}\,\mathrm{d}S_\xi =\\
&\qquad \int_{0S_{Sw}^{(e)}} \left\{(s_1+s_2+s_3)\,\mathbf{n}^{\mathrm{T}}\mathbf{H}_S^{(e)}\right\}\,\mathrm{d}S_\xi + \int_{0S_{Sw}^{(e)}} \tilde{G}\mathbf{n}^{\mathrm{T}}\mathbf{H}_S^{(e)}\,\mathrm{d}S_\xi,\\
&\int_{0S_{Sw}^{(e)}} \frac{\partial G}{\partial n_\xi}\mathbf{H}_F^{(e)}\,\mathrm{d}S_\xi =\\
&\qquad \int_{0S_{Sw}^{(e)}} \frac{\partial\{s_1+s_2+s_3\}}{\partial n_\xi}\mathbf{H}_F^{(e)}\,\mathrm{d}S_\xi + \int_{0S_{Sw}^{(e')}} \frac{\partial\tilde{G}}{\partial n_\xi}\mathbf{H}_F^{(e)}\,\mathrm{d}S_\xi,
\end{aligned} \tag{38}$$

where (e) means the element for the inner integral, $\mathbf{H}_S$ and $\mathbf{H}_F$ are the interpolation matrices for the structural displacement and the fluid velocity potential, respectively, and

$$\begin{aligned}
s_1 &= \frac{1}{\sqrt{r^2+(x_3-\xi_3)^2}},\\
s_2 &= \frac{1}{\sqrt{r^2+(x_3+\xi_3)^2}},\\
s_3 &= -2\frac{\omega^2}{g}e^{\frac{\omega^2}{g}(x_3+\xi_3)}\ln\left\{\sqrt{r^2+(x_3+\xi_3)^2}-(x_3+\xi_3)\right\}.
\end{aligned} \tag{39}$$

When the elements for the outer and inner integrals coincide, the component s_1 reveals singularity, whereas the other components s_2 and s_3 are nearly singular. However, the components s_2 and s_3 also show singularity when the spatial point x_3 and the source point ξ_3 are all equal to zero. Of course, the components s_1, s_2, and s_3 are all nearly singular when the elements for the outer and inner integrals are near each other. The normal derivatives of these components also have similar characteristics.

Accurate and efficient evaluation of these singular and nearly singular integrals is very important because they have a dominant role in constructing the matrices $\mathbf{F}_G$ and $\mathbf{F}_{Gn}$. Actually, such integrals have been well studied, and various numerical methods have been developed. In the case

DOI: 10.1002/nme

of the singular integral, the most widely adopted method is to use the polar coordinate system (see, e.g., Reference [22]). The basic idea of the polar coordinate transformation is that the Jacobian of transformation smooths out the singularity of the components. For nearly singular integrals, Lachat [23] developed a subdivision method where the element is divided into several sub-elements, and in each sub-element, the integral is carried out by the Gaussian quadrature. For a more efficient approach, Telles [22] proposed a nonlinear polynomial coordinate transformation method. This method concentrates the Gauss points on the source point without the subdivision of the elements by third-degree polynomial transformation.

Third, the resulting coefficient matrix of the unknown vector on the left-hand side of Equation (34) is not the Hermitian matrix. In this paper, the well-known flexible generalized minimal residual method [24, 25], which is a kind of projection method that uses a Krylov subspace with variable preconditioning, is used to solve the linear equations.

Finally, because $\mathbf{F}_G$ and $\mathbf{F}_{Gn}$ are dense matrices, their construction and the matrix-vector multiplication in iterative solvers require heavy operations. For example, if the degree of freedom of the nodal velocity potential $\hat{\boldsymbol{\phi}}$ is N, $O(N^2)$ operations are needed for the dense matrix $\mathbf{F}_{Gn}$. In order to reduce such operations, the fast multipole method [26, 27] can be employed. With the use of this novel method, the operations decrease dramatically (for $\mathbf{F}_{Gn}$, e.g., to $O(N)$), resulting in a more efficient and rapid solution procedure. However, the specific procedure and appropriate expansion of the Green's function for the present formulation require further study.

5. MODAL ANALYSIS

For the purpose of reducing the size of the system, we suggest a mode superposition method that uses the eigenvectors of the discrete linear equations for the structural free vibration problem. Beside this advantage, rigid body motion analysis is clearly obtained by using the six rigid body modes.

5.1. Eigenvalue problem of the structure

To establish the basis for the solution vector, the following eigenvalue problem is solved:

$$\mathbf{S}_K \boldsymbol{\psi}_i = \lambda_i \mathbf{S}_M \boldsymbol{\psi}_i; \quad i = 1, 2, \ldots, N, \tag{40}$$

where λ_i is the eigenvalue, $\boldsymbol{\psi}_i$ is the eigenvector, and N is the total degree of freedom for the aforementioned system. The eigenvectors are normalized as

$$\begin{aligned} &\boldsymbol{\psi}_i^{\mathrm{T}} \mathbf{S}_K \boldsymbol{\psi}_j = \lambda_i \delta_{ij}, \quad \text{and} \\ &\boldsymbol{\psi}_i^{\mathrm{T}} \mathbf{S}_M \boldsymbol{\psi}_j = \delta_{ij}, \quad \text{except for the rigid body modes.} \end{aligned} \tag{41}$$

Then, we can approximate the nodal displacement vector as

$$\begin{aligned} \hat{\mathbf{u}} &\approx q_1 \boldsymbol{\psi}_1 + q_2 \boldsymbol{\psi}_2 + \ldots + q_{N_a} \boldsymbol{\psi}_{N_a} \\ &= \boldsymbol{\Psi} \mathbf{q}, \end{aligned} \tag{42}$$

where N_a is the number of eigenvectors for approximation, $\mathbf{q}$ is the generalized coordinate vector, and $\boldsymbol{\Psi} = [\boldsymbol{\psi}_1, \boldsymbol{\psi}_2, \ldots, \boldsymbol{\psi}_{N_a}]$.

Because Equation (40) comes from the free vibration equation without any constraints, the stiffness matrix $\mathbf{S}_K$ is the positive semidefinite matrix. Thus, there are six zero eigenvalues and corresponding eigenvectors. Note that in the present formulation, the modes are the dry modes of the deformed structure in the static equilibrium state.

5.2. Reduced linear system of equations

If we orthonormalize the rigid body modes with respect to the mass matrix $\mathbf{S}_M$ and apply Equation (42) into Equation (34), then the part of the structural equation after being multiplied by $\boldsymbol{\Psi}^{\mathrm{T}}$ is

$$-\omega^2 \mathbf{I}\mathbf{q} + \boldsymbol{\Lambda}\mathbf{q} + \boldsymbol{\Psi}^{\mathrm{T}} (\mathbf{S}_{KN} - \mathbf{S}_{HD} - \mathbf{S}_{HN}) \boldsymbol{\Psi}\mathbf{q} - j\omega \boldsymbol{\Psi}^{\mathrm{T}} \mathbf{S}_D \hat{\boldsymbol{\phi}} = 0, \tag{43}$$

DOI: 10.1002/nme

where

$$I_{ij} = \delta_{ij}, \quad \Lambda_{ij} = \lambda_i \delta_{ij}; \quad i, j = 1, 2, \ldots, N_a. \tag{44}$$

Then, the modified equation is

$$\begin{bmatrix} -\omega^2 \mathbf{I} + \mathbf{\Lambda} + \mathbf{\Psi}^{\mathrm{T}} (\mathbf{S}_{KN} - \mathbf{S}_{HD} - \mathbf{S}_{HN}) \mathbf{\Psi} & -j\omega \mathbf{\Psi}^{\mathrm{T}} \mathbf{S}_D \\ j\omega \mathbf{F}_G \mathbf{\Psi} & \alpha \mathbf{F}_M - \mathbf{F}_{Gn} \end{bmatrix} \begin{bmatrix} \mathbf{q} \\ \hat{\boldsymbol{\phi}} \end{bmatrix} = \begin{bmatrix} 0 \\ 4\pi \mathbf{R}_I \end{bmatrix}. \tag{45}$$

5.3. Hydrodynamic rigid body motion analysis for the steady state

The hydrodynamic rigid body motion analysis can be derived from the formulation proposed. The basic condition is that the linear strain tensor is equal to zero in Equation (30). Thus, the matrix $\mathbf{S}_K$ in Equation (34) is automatically zero. We can express the displacement field of rigid body motions about the origin of the Cartesian coordinate system, surge, sway, heave, roll, pitch, and yaw, as

$$\begin{aligned} u_i^{R1} &= q_1^R \delta_{1i}, \quad u_i^{R2} = q_2^R \delta_{2i}, \quad u_i^{R3} = q_3^R \delta_{3i}, \\ u_i^{R4} &= q_4^R \varepsilon_{ijk} \delta_{1j}\, {}^0x_k, \\ u_i^{R5} &= q_5^R \varepsilon_{ijk} \delta_{2j}\, {}^0x_k, \\ u_i^{R6} &= q_6^R \varepsilon_{ijk} \delta_{3j}\, {}^0x_k, \end{aligned} \tag{46}$$

where ε_{ijk} is the permutation symbol.

We modify the initial stress-related term in Equation (30) as

$$\int_{{}^0V_S} {}^0\sigma_{ij} \bar{\eta}_{ij} \, \mathrm{d}V = \int_{{}^0V_S} {}^0\sigma_{ij} \frac{\partial u_k}{\partial {}^0x_i} \frac{\partial \bar{u}_k}{\partial {}^0x_j} \, \mathrm{d}V \tag{47a}$$

$$= \int_{{}^0S_{S_w}} {}^0\sigma_{ij}\, {}^0n_j \frac{\partial u_k}{\partial {}^0x_i} \bar{u}_k \, \mathrm{d}S - \int_{{}^0V_S} \frac{\partial {}^0\sigma_{ij}}{\partial {}^0x_j} \frac{\partial u_k}{\partial {}^0x_i} \bar{u}_k \, \mathrm{d}V - \int_{{}^0V_S} {}^0\sigma_{ij} \frac{\partial^2 u_k}{\partial {}^0x_j \partial {}^0x_i} \bar{u}_k \, \mathrm{d}V \tag{47b}$$

$$= \int_{{}^0S_{S_w}} \rho_w g\, {}^0x_3\, {}^0n_i \frac{\partial u_k}{\partial {}^0x_i} \bar{u}_k \, \mathrm{d}S - \int_{{}^0V_S} {}^0\rho_s g \frac{\partial u_k}{\partial {}^0x_3} \bar{u}_k \, \mathrm{d}S, \tag{47c}$$

where we apply the symmetry of the Cauchy stress tensor (Equation (47a)), the divergence theorem (Equation (47b)), and the zero linear strain tensor condition and Equation (3) at time 0 (Equation (47c)). A similar derivation of Equation (47c) can also be found in Reference [11]. The matrix formulas for these terms are then

$$\begin{aligned} \int_{{}^0S_{S_w}} \rho_w g\, {}^0x_3\, {}^0n_i \frac{\partial u_k}{\partial {}^0x_i} \bar{u}_k \, \mathrm{d}S &= \hat{\bar{\mathbf{u}}}^{\mathrm{T}} \mathbf{S}_{HS} \hat{\mathbf{u}}, \\ \int_{{}^0V_S} {}^0\rho_s g \frac{\partial u_k}{\partial {}^0x_3} \bar{u}_k \, \mathrm{d}S &= \hat{\bar{\mathbf{u}}}^{\mathrm{T}} \mathbf{S}_{HB} \hat{\mathbf{u}}. \end{aligned} \tag{48}$$

Thus, we obtain the following linear system of equations for the rigid body motion analysis in the steady state:

$$\begin{bmatrix} \mathbf{\Psi}^{R\mathrm{T}} \left(-\omega^2 \mathbf{S}_M + \mathbf{S}_{HS} - \mathbf{S}_{HB} - \mathbf{S}_{HD} - \mathbf{S}_{HN}\right) \mathbf{\Psi}^R & -j\omega \mathbf{\Psi}^{R\mathrm{T}} \mathbf{S}_D \\ j\omega \mathbf{F}_G \mathbf{\Psi}^R & \alpha \mathbf{F}_M - \mathbf{F}_{Gn} \end{bmatrix} \begin{bmatrix} \mathbf{q}^R \\ \hat{\boldsymbol{\phi}} \end{bmatrix} = \begin{bmatrix} 0 \\ 4\pi \mathbf{R}_I \end{bmatrix}, \tag{49}$$

where

$$\mathbf{\Psi}^R \mathbf{q}^R = q_1^R \boldsymbol{\psi}_1^R + \ldots + q_6^R \boldsymbol{\psi}_6^R, \tag{50}$$

in which $\boldsymbol{\psi}_i^R$ $(i = 1, 2, \ldots, 6)$ means the nodal displacement vector for the ith rigid body mode.

DOI: 10.1002/nme

6. COMPARISON WITH CONVENTIONAL FORMULATION

The conventional and present formulations are described in Table I. In particular, it is emphasized that the solution procedure of the present formulation is simpler than the conventional formulation where four steps are required. In the present formulation, solving the coupled equation is just needed, and when desired mainly for computational efficiency, the modal analysis can be included.

Table II shows the comparison of primary terms between the conventional and present formulations. In the present method, added mass, radiated wave damping, and wave excitation forces are put into the single interaction term $\mathbf{S}_D$. Contrary to the conventional method, the interaction term is more easily constructed, and the components of it are more sparsely stored. Thus, the computational algorithm is more efficient.

For the hydrostatic stiffness, various formulations have been proposed in the conventional formulation (see, e.g., References [6, 11, 28]). In those, our formulation is the same as the one suggested by Huang and Riggs [11], if it is expressed in the generalized coordinates. These two formulations are complete in that they contain exact hydrostatic pressure stiffness and geometric stiffness.

Table I. Comparison between the conventional and present formulations: solution procedure.

A. Conventional formulation

Step 1. Find structural dry or mathematical modes:

$$\mathbf{u} \approx \Sigma g_i \boldsymbol{\mu}_i$$

where $g_i, \boldsymbol{\mu}_i$: generalized coefficients and basis functions for ith structural mode

Step 2. Solve diffraction and radiation problems:

(a) Diffraction problem: $\alpha\phi^D - ⨍_{0S_{S_w}} \partial G/\partial n \phi^D \, \mathrm{d}S_\xi = 4\pi\phi^I$

(b) Radiation problem: $\alpha\phi_i^R - ⨍_{0S_{S_w}} \left\{\partial G/\partial n \phi_i^R - G\partial\phi_i^R/\partial n\right\} \, \mathrm{d}S_\xi = 0$

where ϕ^D: diffraction velocity potential (diffracted and scattered waves)

ϕ_i^R: radiation velocity potential for ith structural mode (radiated wave by ith structural mode)

Step 3. Calculate interaction coefficients:

$$F_i = j\omega\rho_w \int_{0S_{S_w}} \phi^D \boldsymbol{\mu}_i \cdot \mathbf{n} \, \mathrm{d}S$$

$$A_{ij} = -1/\omega^2 \times \mathrm{Re}\left\{-j\omega\rho_w \int_{0S_{S_w}} \phi_j^R \boldsymbol{\mu}_i \cdot \mathbf{n} \, \mathrm{d}S\right\}$$

$$C_{ij} = 1/\omega \times \mathrm{Im}\left\{-j\omega\rho_w \int_{0S_{S_w}} \phi_j^R \boldsymbol{\mu}_i \cdot \mathbf{n} \, \mathrm{d}S\right\}$$

where $\mathbf{F}$: generalized coefficient vector for wave excitation forces

$\mathbf{A}, \mathbf{C}$: generalized coefficient matrices for added mass and radiated wave damping

Step 4. Solve generalized equations of motion:

$$[-\omega^2(\mathbf{M}+\mathbf{A}) + j\omega\mathbf{C} + \mathbf{K}_S + \mathbf{K}_H]\mathbf{g} = \mathbf{F}$$

where $\mathbf{M}, \mathbf{K}_S, \mathbf{K}_H$: generalized coefficient matrices for structural mass and stiffness and hydrostatic stiffness

B. Present formulation

Step 1. Find structural dry modes (optional):

$$\hat{\mathbf{u}} \approx \Sigma q_i \boldsymbol{\psi}_i$$

Step 2. Solve discrete coupled equations:

$$\begin{bmatrix} -\omega^2\mathbf{S}_M + \mathbf{S}_K + \mathbf{S}_{KN} - \mathbf{S}_{HD} - \mathbf{S}_{HN} & -j\omega\mathbf{S}_D \\ j\omega\mathbf{F}_G & \alpha\mathbf{F}_M - \mathbf{F}_{Gn} \end{bmatrix} \begin{bmatrix} \hat{\mathbf{u}} \\ \hat{\boldsymbol{\phi}} \end{bmatrix} = \begin{bmatrix} 0 \\ 4\pi\mathbf{R}_I \end{bmatrix}$$

Table II. Comparison between the conventional and present formulations: primary terms.

	Conventional formulation	Present formulation
Unknown variables	$\phi^D, \phi_i^R, \mathbf{g}$	$\hat{\mathbf{u}}, \hat{\boldsymbol{\phi}}$
Interaction coefficients	$\mathbf{A}, \mathbf{C}, \mathbf{F}$	$\mathbf{S}_D$
Hydrostatic stiffness coefficient	$\mathbf{K}_H$ (Price and Wu [6], Newman [28], and Huang and Riggs [11])	$\mathbf{S}_{KN} - \mathbf{S}_{HD} - \mathbf{S}_{HN}$

DOI: 10.1002/nme

7. HARMONIC EXCITATION SURFACE FORCES

In this section, we consider surface forces that act on floating structures, which are not wave excitation forces. The modeling of general surface forces depends on their characteristics, but in this study, we focus on harmonic surface forces that do not vary according to their position.

The external energy due to the harmonic excitation surface force with angular frequency ω can be modeled as

$$\int_{0S_{S_f}} f_i \bar{u}_i \, \mathrm{d}S = \hat{\mathbf{u}}^{\mathrm{T}} \mathbf{R}_f, \tag{51}$$

where ${}^t f_i = \mathrm{Re}\left\{ f_i \left({}^0\mathbf{x}\right) e^{j\omega t} \right\}$, ${}^t f_i$ is the harmonic excitation force per unit surface area and the force is applied to the surface S_{S_f}.

The resultant discrete equation for the radiation problems of floating structures subjected to harmonic excitation surface forces is the same as Equation (34), except for the force vector, the right-hand side of the equation, which we denote as $\mathbf{R}$. The force vector then becomes

$$\mathbf{R} = \begin{bmatrix} \mathbf{R}_f \\ 0 \end{bmatrix}. \tag{52}$$

8. NUMERICAL EXAMPLES

We solve three different hydroelastic problems and present the numerical results. The first and second problems deal with interactions between floating structures and incident waves, and the last model concerns a floating structure subjected to a harmonic point load as well as an incident wave. The solutions of the first and second problems are compared with the experimental results and with the numerical results of available computer programs, respectively.

WAMIT is a well-developed computer program for the hydrodynamic rigid body motion analysis of floating structures. HYDRAN is a computer program that analyzes the hydroelastic response of floating structures. The basic approach in HYDRAN was developed by Wu [5] and Price and Wu [6], and it uses the constant panel method to solve the fluid equation. These two programs employ the conventional formulation, and HYDRAN uses the formulation proposed by Huang and Riggs [11] for the hydrostatic stiffness.

In all the numerical examples, the density of water ρ_w is 1000 $\mathrm{kg/m^3}$, and the acceleration of gravity g is 9.8 $\mathrm{m/s^2}$. The water depth h is assumed to be finite for the floating plate problem and to be infinite for the other problems. We use the four-node Mixed Interpolation of Tensorial Components (MITC) shell finite elements developed by Dvorkin and Bathe [29]. The MITC finite element is a well-known shell finite element that effectively alleviates the shear locking phenomena

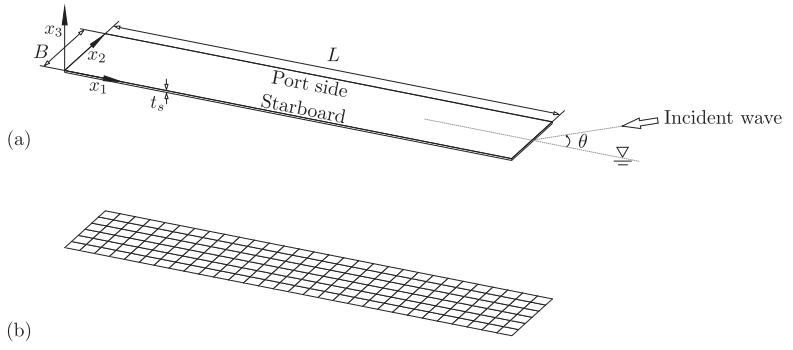

Figure 4. Floating plate problem: (a) problem description and (b) finite and boundary element meshes used (identical mesh is used for the structure and fluid boundary surface).

DOI: 10.1002/nme

(see, e.g., References [29–35]). For the fluid boundary element, a four-node quadrilateral element is used, and as for the structural element, the isoparametric interpolation method is adopted for the fluid velocity potential and fluid boundary surface geometry. Also, for simplicity, we use 2π instead of α in Equations (45) and (49). Because most parts of the wet surfaces of the models used are smooth, the influence of this replacement on the solutions is negligible.

The full dry modes are used in the first problem, whereas, in the other problems, the mode superposition method is used to only include the dry modes of floating structures that correspond to the natural frequencies below $\sqrt{1000}\,\mathrm{rad/s}$.

In the second and last problems, we assume the initial configuration as the hydrostatic equilibrium state of the rigid body case and use this configuration for the reference configuration of hydrodynamic analysis. Of course, we perform a hydrostatic analysis to include the geometric stiffness.

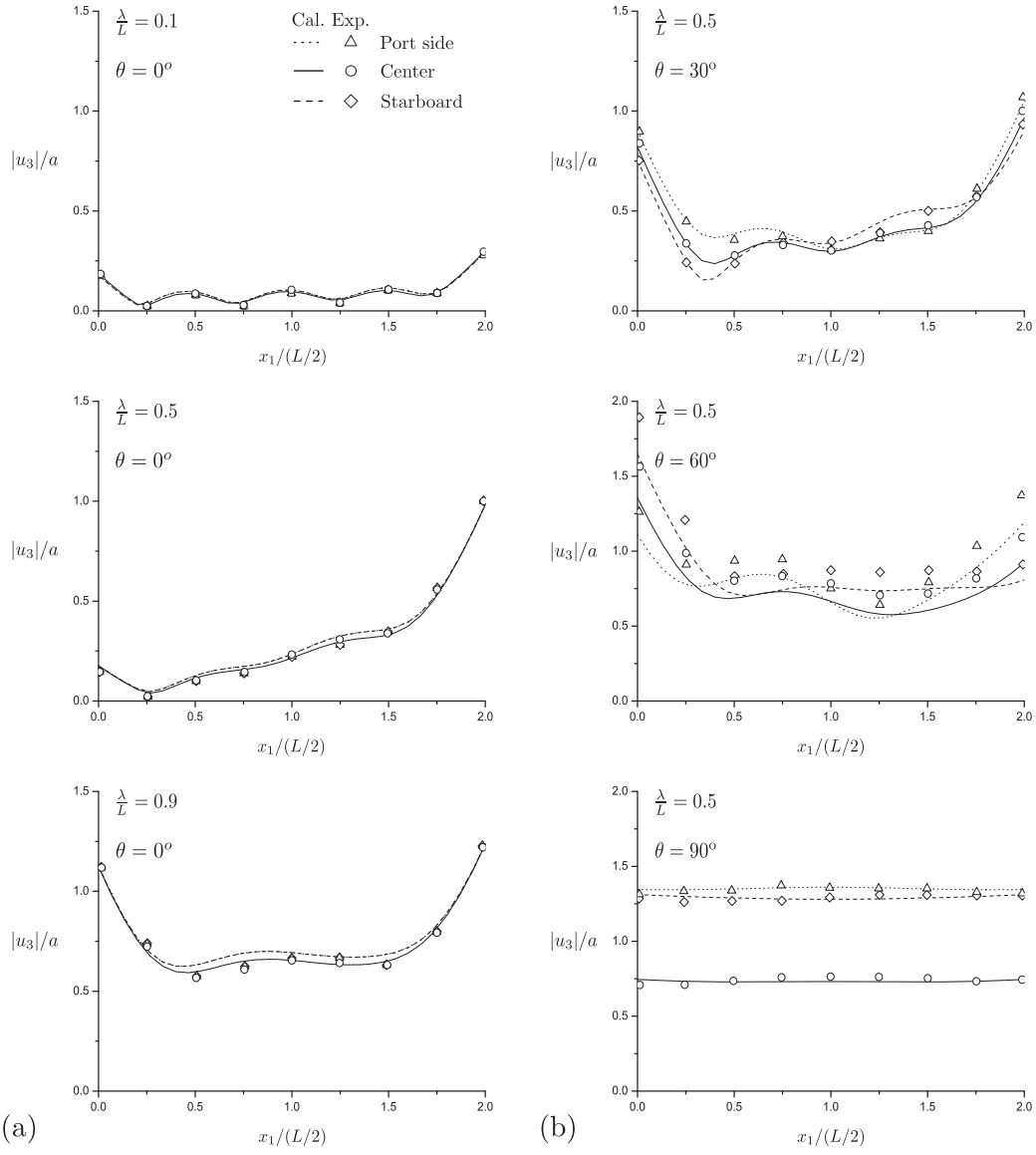

Figure 5. Vertical displacement distribution along the center, port side, and starboard lines of the floating flexible plate: (a) when λ/L varies and $\theta = 0^o$ and (b) when $\lambda/L = 0.5$ and θ varies.

DOI: 10.1002/nme

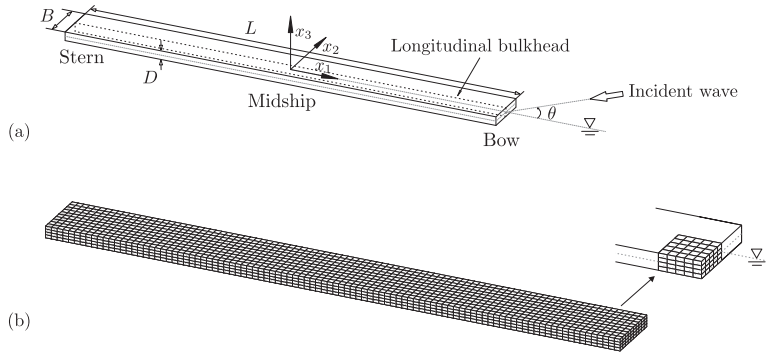

Figure 6. Floating barge problem: (a) problem description and (b) finite and boundary element meshes used.

Table III. Thickness and density distributions of the floating barge.

	Top deck	Bottom deck	Side hull	Bulkhead
Thickness t_s (m)	0.005	0.02	0.02	0.005
Density ρ_s (kg/m^3)	1.0×10^3	3.3389×10^4	3.3389×10^4	3.3389×10^4

However, we do not use an iterative solution method because, in this case, the nonlinear effects are negligible (the displacement $\overset{0}{\underset{0}{u}}_i$ and the change of the wet surface are small).

8.1. A floating plate interacting with an incident wave

Yago and Endo conducted a hydroelastic experiment using a floating plate model (length L is 9.75 m, breadth B is 1.9 m, thickness t_s is 5.45 cm, draft d is 1.67 cm, bending stiffness EI is 1.788×10^3 kgf$\cdot$m^2, and water depth h is 1.9 m) [36]. In order to validate the formulation proposed, we analyze the floating plate problem and compare the numerical solutions with the experimental results.

For simplicity, we assume that the draft is zero. Thus, hydrostatic analysis is not required, and the matrices $\mathbf{S}_{KN}$ and $\mathbf{S}_{HN}$ in Equation (34) are automatically zero.

The floating plate is modeled by a 30 (in length) $\times$ 6 (in breadth) mesh of shell finite elements, and the same mesh is used for the fluid boundary elements on the interface boundary surface. We use full dry modes of the plate; that is, the mode superposition technique is not used. We compute the hydroelastic response of the floating plate problem by varying the incident wavelength λ when the incident wave angle θ is zero. In the case that the wavelength is half the plate's length, numerical calculations are performed by increasing the incident angle θ by 30^o to 90^o.

Figure 4 shows the description of the plate model, and Figure 5 represents the comparison between the numerical results and the experimental results. Overall, the numerical results have good agreement with the experiments.

8.2. A floating barge interacting with an incident wave

Let us consider the floating barge problem shown in Figure 6. The barge's dimensions are the same with the one used in the eference [37]; that is, the length L is 100 m, the breadth B is 10 m, and the depth D is 2 m. However, a longitudinal bulkhead is additionally located along the centerline in the model. The thickness and density distribution given in Table III ensures that the draft d is 1 m in the hydrostatic equilibrium state of the rigid body case.

DOI: 10.1002/nme

Table IV. Hydrostatic stiffness coefficients for the floating rigid barge.

Hydrostatic stiffness coefficients	Analytic values	Computed values
$S^R_{H,33}$ (N/m)	9.8000E+06	9.8000E+06
$S^R_{H,44}$ (N · m)	8.3262E+07	8.3262E+07
$S^R_{H,55}$ (N · m)	8.1683E+09	8.1683E+09

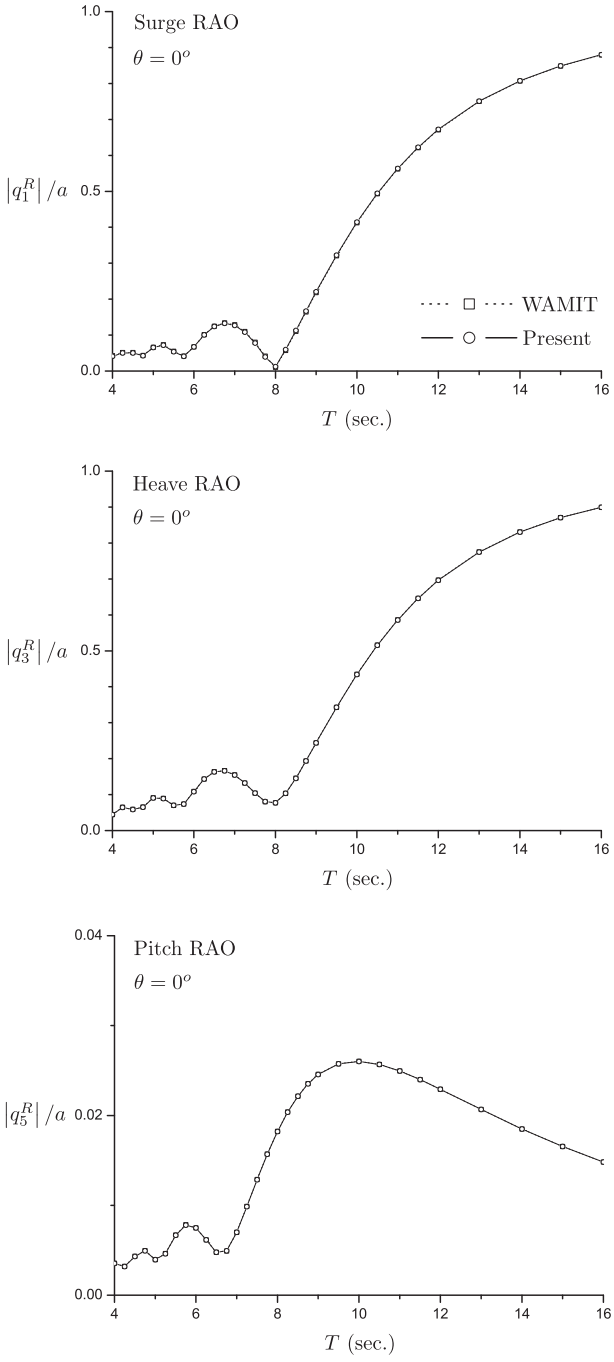

Figure 7. Response amplitude operators of the surge, heave, and pitch motions of the floating rigid barge when $\theta = 0^o$.

DOI: 10.1002/nme

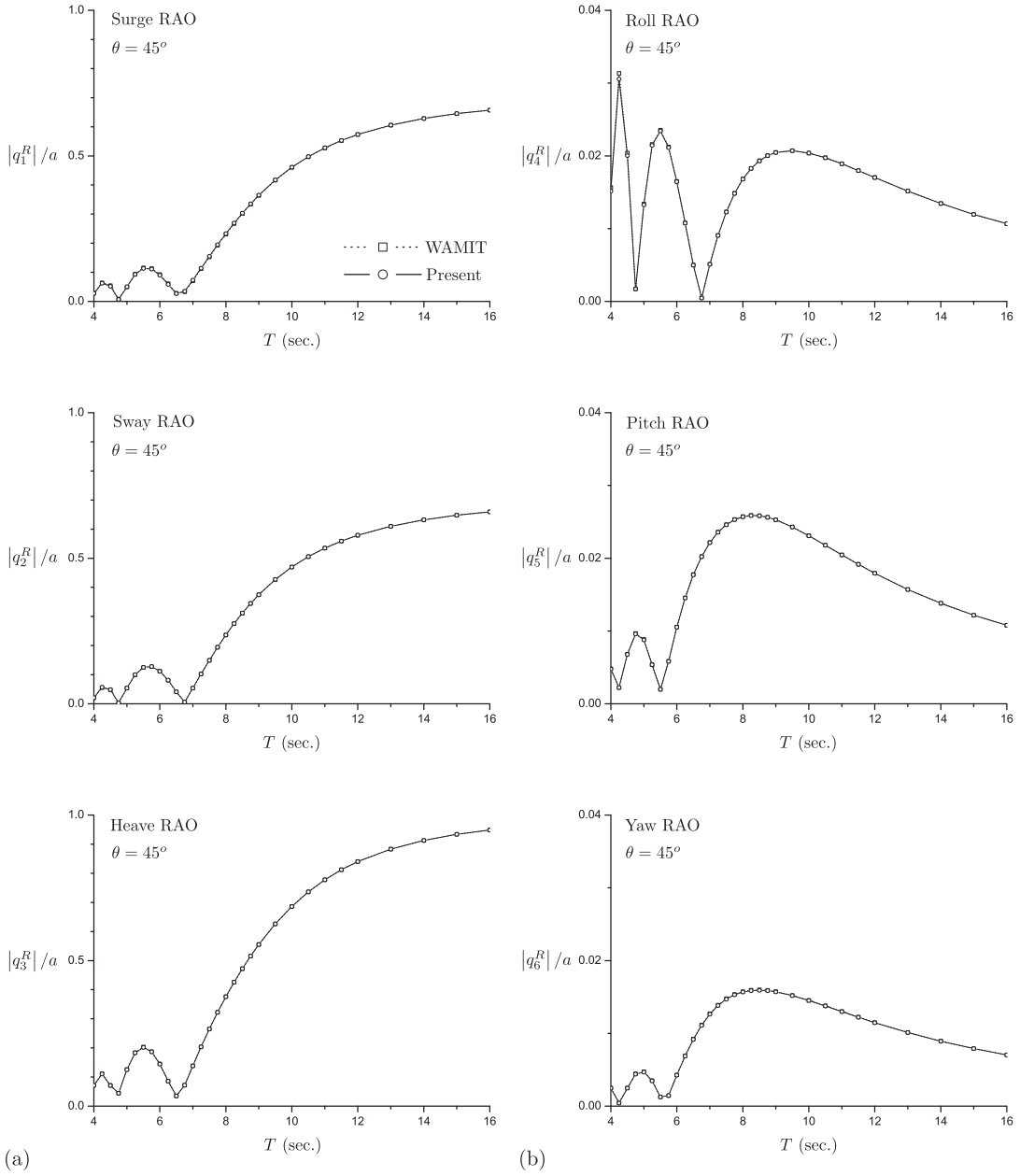

Figure 8. Response amplitude operators of the floating rigid barge when $\theta = 45^o$: (a) the surge, sway, and heave motions, and (b) the roll, pitch, and yaw motions.

For the barge model, 100, 10, and 4 shell finite elements are used in the length, breadth, and depth directions, respectively. The fluid boundary surface is meshed to match the structural elements; that is, 100, 10, and 2 fluid boundary elements are used in the length, breadth, and depth direction, respectively.

In the rigid body case, there is an analytic solution for the hydrostatic stiffness [10]. When the origin of the coordinate system is placed on the center of flotation, as shown in Figure 6, the component of hydrostatic stiffness matrix for the rectangular barge, which is denoted as $\mathbf{S}_H^R$, is defined by

DOI: 10.1002/nme

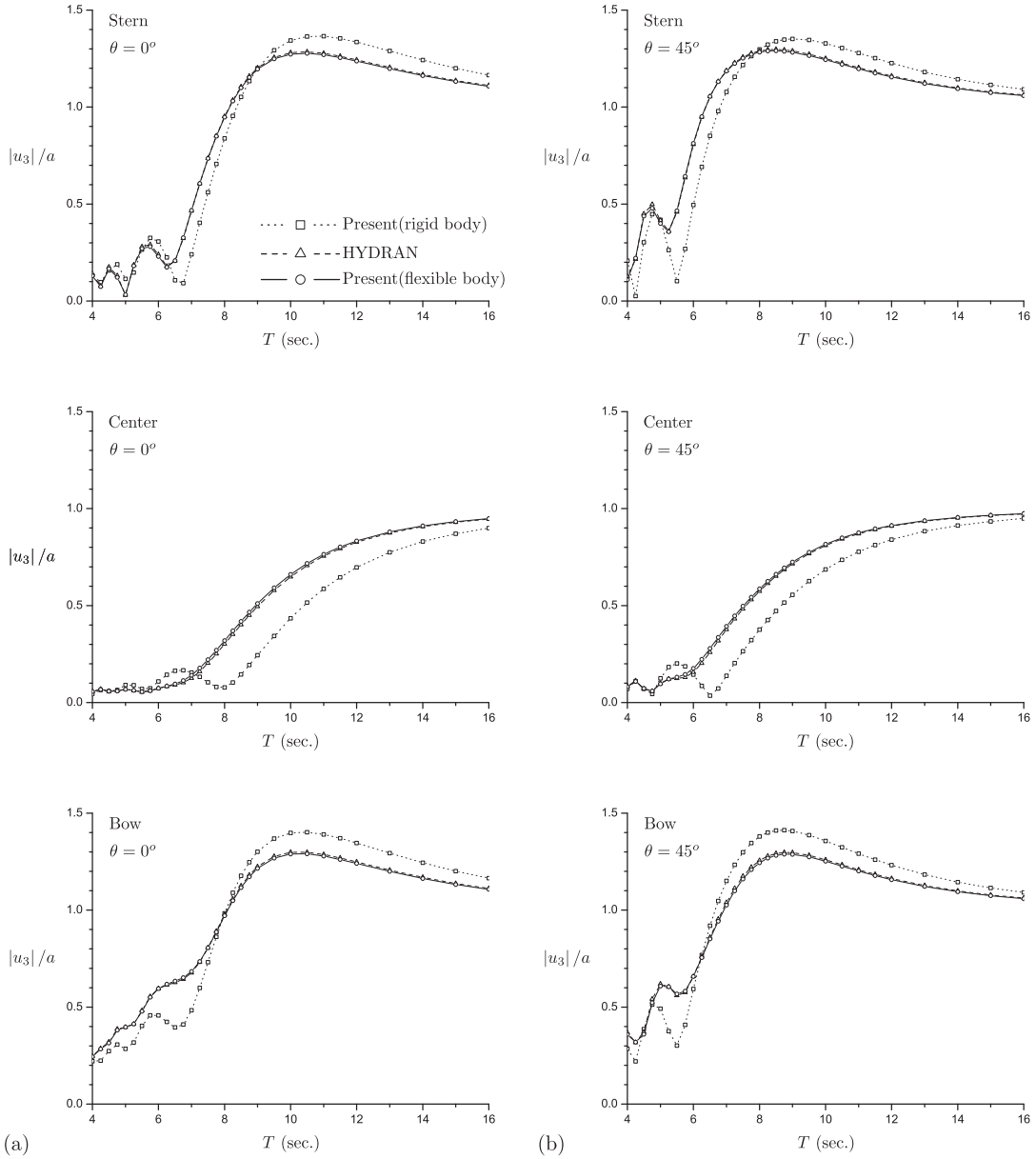

Figure 9. Vertical displacement (center of breadth) at the stern, center, and bow of the top deck of the floating rigid and flexible barge: (a) when $\theta = 0^o$ and (b) when $\theta = 45^o$.

$$
\begin{aligned}
S^R_{H,33} &= \rho_w g L B \\
S^R_{H,44} &= \frac{1}{12}\rho_w g L B^3 + x_3^b \rho_w g L B d - x_3^g m_s g \\
S^R_{H,55} &= \frac{1}{12}\rho_w g L^3 B + x_3^b \rho_w g L B d - x_3^g m_s g \\
S^R_{H,ij} &= 0 \quad \text{for the other components;} \quad i, j = 1, 2, \ldots, 6
\end{aligned} \tag{53}
$$

where x_i^b is the center of buoyancy, x_i^g is the structural center of gravity, and m_s is the structural mass. The subscripts, $1, 2, \ldots, 6$, mean the generalized coordinates for the rigid body motions about the spatially fixed coordinate x_i, that is, surge, sway, heave, roll, pitch, and yaw, respectively.

DOI: 10.1002/nme

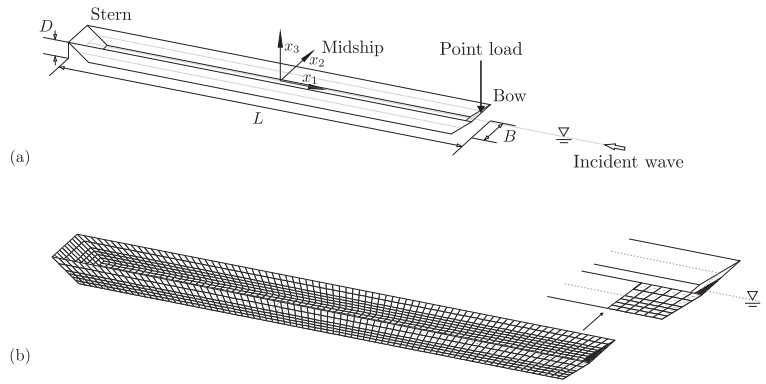

Figure 10. Floating hull problem: (a) problem description and (b) finite and boundary element meshes used.

Table IV shows that the formulation proposed in this study produces exact hydrostatic stiffness coefficients.

Using Equation (49), we performed the hydrodynamic rigid body motion analysis, and Figures 7 and 8 show response amplitude operators corresponding to two different incident angles (0^o and 45^o). The results are compared with those of WAMIT. In the figures, T means the period of the incident wave. For the numerical results of WAMIT, the higher-order method (fourth-order B-spline functions) is used, and the numbers of panels used are 20, 8, and 2 in the length, breadth, and depth directions, respectively. The results of the present formulation are almost identical to those of WAMIT.

Using elastic modulus $E = 100\text{GPa}$, and Poisson's ratio $\nu = 0.3$, we performed the hydroelastic analysis. Figure 9 represents the numerical results compared with those of HYDRAN. To investigate the effect of hydroelasticity, we also plot the numerical results of the proposed formulation for the rigid body case.

8.3. A floating hull interacting with an incident wave and a harmonic point load

In this example, we consider a floating hull subjected to an incident wave and a harmonic point load, as shown in Figure 10. The stern and bow of the hull is equally sloped linearly, and we remove the top deck of the hull in order to make the model more flexible. The load is applied to the center of top edge of the bow.

The length L is 100 m at the top and 90 m at the bottom, and the depth D is 4 m. The thickness t_s is 0.03 m, and the density ρ_s is $6.3585 \times 10^4\ \text{kg/m}^3$ at the bottom plate and $5.0 \times 10^4\ \text{kg/m}^3$ at the other sides. This density distribution results in the draft $d = 2$ m in the hydrostatic equilibrium state of the rigid body case. The elastic modulus $E = 200\ \text{GPa}$ and Poisson's ratio $\nu = 0.3$ are used. For the harmonic point load, we set the magnitude and phase of it as 500 kN and 0^o, respectively.

The numbers of shell finite elements used are 80, 10, and 6 in the length, breadth, and depth directions, respectively (two elements above the free surface and four elements below the free surface). To satisfy the matching condition with the structural elements, we divide the fluid boundary surface into 80, 10, and 4 elements in the length, breadth, and depth directions, respectively.

In this case, the displacement can be expressed as

$$\begin{aligned} {}^t_0u_i &= \text{Re}\left\{|u_i^I|e^{j(\omega_I t+\vartheta_I)} + |u_i^f|e^{j(\omega_f t+\vartheta_f)}\right\} \\ &= \sqrt{|u_i^I|^2 + |u_i^f|^2 + 2|u_i^I||u_i^f|\cos((\omega_f-\omega_I)t+\vartheta_f-\vartheta_I)}\times \\ &\quad \cos\left(\omega_I t + \vartheta_I + \arctan\frac{|u_i^f|\sin((\omega_f-\omega_I)t+\vartheta_f-\vartheta_I)}{|u_i^I| + |u_i^f|\cos((\omega_f-\omega_I)t+\vartheta_f-\vartheta_I)}\right), \end{aligned} \tag{54}$$

DOI: 10.1002/nme

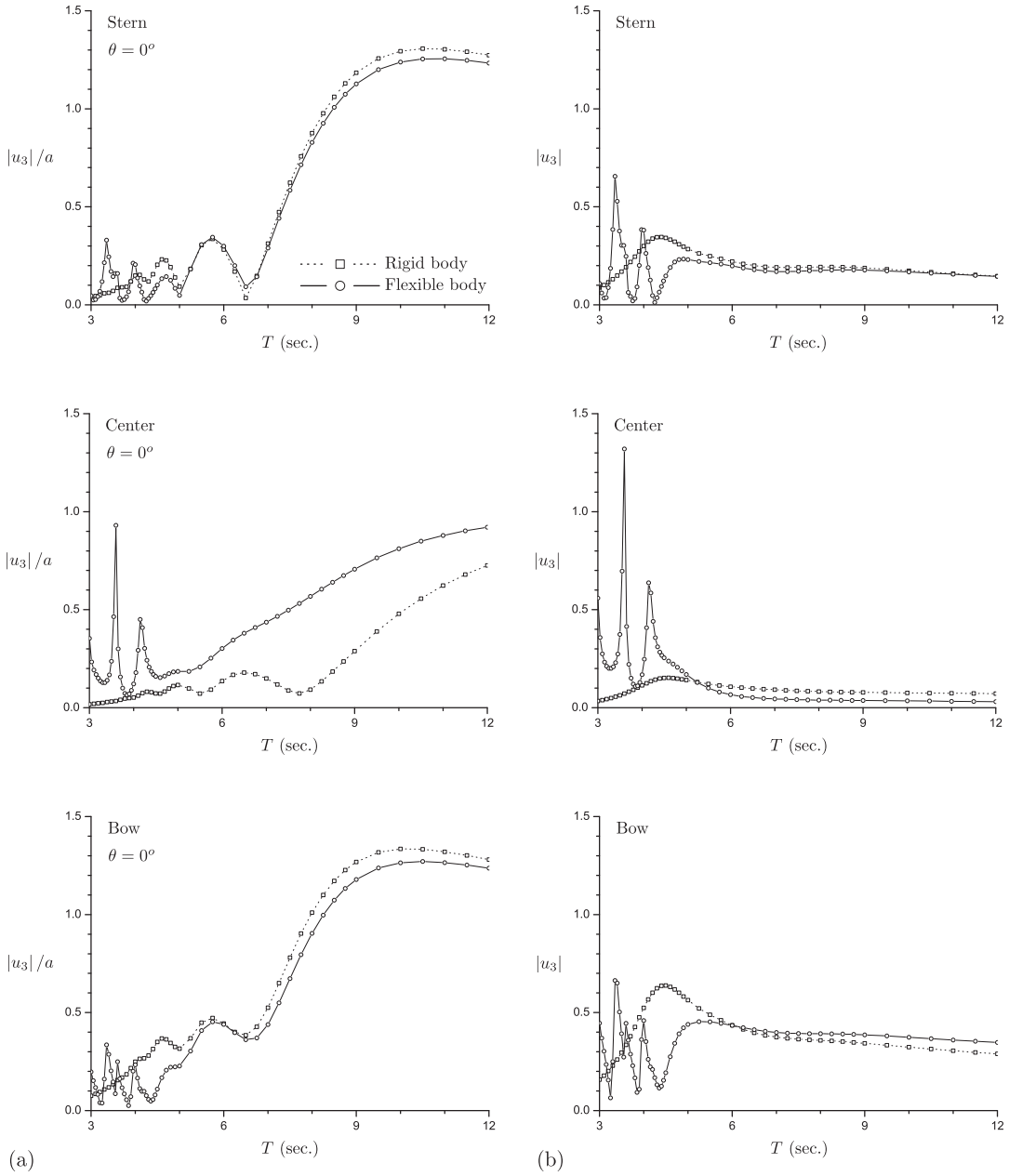

Figure 11. Vertical displacement (center of breadth) at the stern, center, and bow of the bottom plate of the floating rigid and flexible hull: (a) when an incident wave is applied and (b) when a harmonic point load is applied.

where ϑ is the phase of displacement u_i and the superscript or subscript I and f mean the attributions of incident wave and point load, respectively.

We first evaluate the displacement of the rigid and flexible models when the incident wave and the point load are applied individually. Figure 11 shows the results.

For the steady state behavior of the hull interacting with the harmonic point load, as well as an incident wave, we calculate it when the periods of incident waves are 3.58, 6.20, and 8.01 s ($\lambda/L = 0.2, 0.6, 1.0$), whereas the period of point load is fixed at 4 s. Figure 12 represents the calculated displacements of the three cases.

DOI: 10.1002/nme

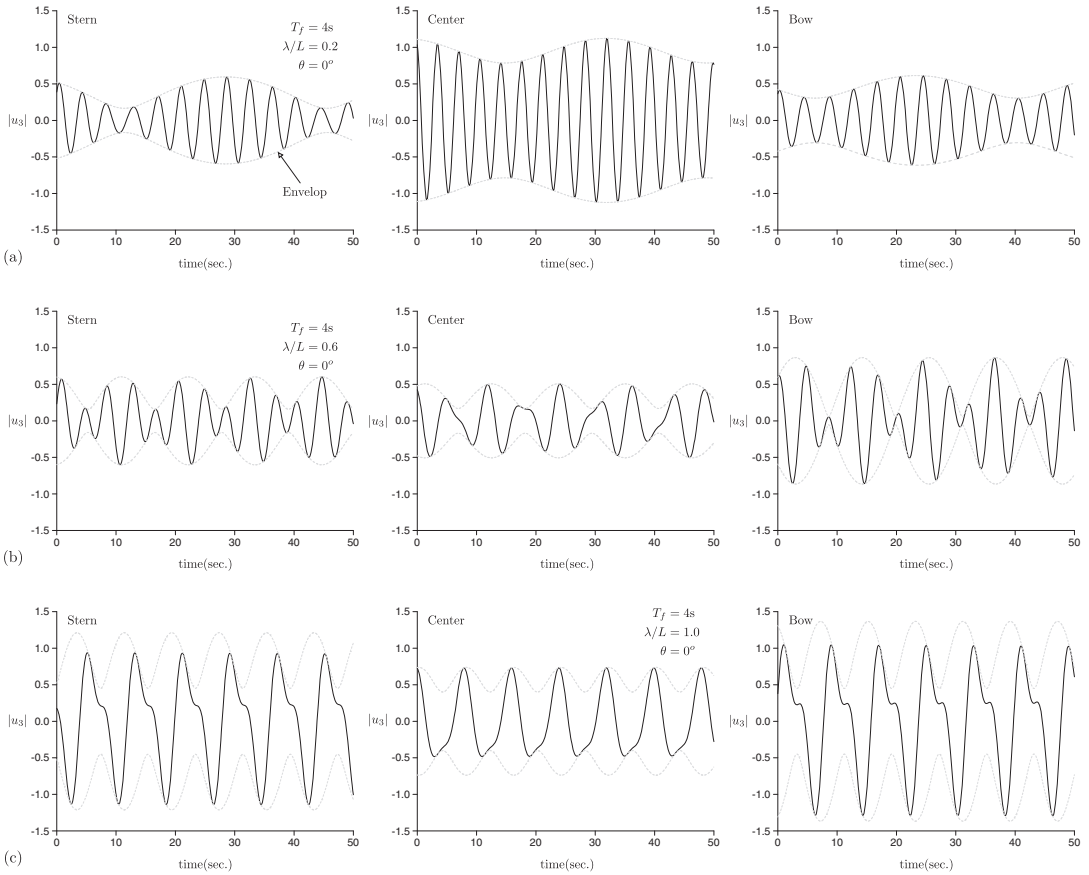

Figure 12. Vertical displacement (center of breadth) and corresponding envelope (dashed gray line) at the stern, center, and bow of the bottom plate of the floating flexible hull interacting with an incident wave as well as a point load: (a) when $\lambda/L = 0.2$ ($T_I \approx 3.58$s) and $T_f = 4$s, (b) when $\lambda/L = 0.6$ ($T_I \approx 6.20$s) and $T_f = 4$s, and (c) when $\lambda/L = 1.0$ ($T_I \approx 8.01$s) and $T_f = 4$s.

9. CONCLUSIONS

In this paper, we derived a formulation for the general 3D hydroelastic analysis of floating structures subjected to surface regular waves as well as other excitation forces. The structural formulation is based on the nonlinear finite element procedure. For the fluid modeling, the total potential-based boundary element method is employed and directly coupled with the structural formulation. The formulation is mathematically clear and complete as well. The complete hydrostatic stiffness and all the interaction terms are included in the formulation, and hydrostatic and hydrodynamic problems can be represented in a unified manner. By applying the additional condensation procedure in conjunction with the modal superposition method, the present formulation can be linked to the conventional wave-structure interaction formulation. The major advantages of the present formulation are simplicity and straightforwardness compared with the conventional formulation.

As numerical examples, we solved the problems of floating plate and barge interacting with an incident wave and the radiation problem of floating hull subjected to a harmonic point load. The numerical results corroborate the high fidelity of the present formulation when compared with the experimental results and the numerical results of existing commercial codes based on the conventional formulation.

Future works that extend the present formulation would include cable-moored floating structures, moving floating structures, and transient analysis capabilities for the nonlinearity of floating structures and surface waves.

DOI: 10.1002/nme

ACKNOWLEDGEMENTS

This work was supported by the Basic Science Research Program through the National Research Foundation of Korea (NRF) funded by the Ministry of Education, Science and Technology (No. 2011-0014387) and also by the WCU (World Class University) Program through the Korea Science and Engineering Foundation funded by the Ministry of Education, Science and Technology, Republic of Korea (Grant Number R31-2008-000-10045-0).

REFERENCES

1. John F. On the motion of floating bodies I. *Communications on Pure and Applied Mathematics* 1949; **2**(1):13–57.
2. John F. On the motion of floating bodies II. *Simple harmonic motions, Communications on Pure and Applied Mathematics* 1950; **3**(1):45–101.
3. Watanabe E, Utsunomiya T, Wang CM. Hydroelastic analysis of pontoon-type VLFS: a literature survey. *Engineering Structures* 2004; **26**(2):245–256.
4. Bishop RED, Price WG. *"Hydroelasticity of Ships"*. Cambridge University Press: Cambridge, UK, 1979.
5. Wu Y. "Hydroelasticity of floating bodies". *Ph.D Thesis*, Brunel University: Uxbridge, UK, 1984.
6. Price WG, Wu Y. "Hydroelasticity of marine structures". In *Theoretical and Applied Mechanics*, Niordson FI, Olhoff N (eds). Elsevier Science Publishers B.V.: Amsterdam, The Netherlands, 1985; 311–337.
7. Khabakhpasheva TI, Korobkin AA. Hydroelastic behaviour of compound floating plate in waves. *Journal of Engineering Mathematics* 2002; **44**:21–40.
8. Wang CD, Meylan MH. A higer-order-coupled boundary element and finite element method for the wave forcing of a floating elastic plate. *Journal of Fluids and Structures* 2004; **19**(4):557–572.
9. Eatock Taylor R. Hydroelastic analysis of plates and some approximations. *Journal of Engineering Mathematics* 2007; **58**:267–278.
10. Newman JN. *Marine Hydrodynamics*. The MIT Press: Cambridge, Massachusetts, U.S.A., 1977.
11. Huang LL, Riggs HR. The hydrostatic stiffness of flexible floating structures for linear hydroelasticity. *Marine Structures* 2000; **13**(2):91–106.
12. Bathe KJ. *Finite Element Procedures*. Prentice Hall: Englewood Cliffs, New Jersey, U.S.A., 1996.
13. Schweizerhof K, Ramm E. Displacement dependent pressure loads in nonlinear finite element analyses. *Computers & Structures* 1984; **18**(6):1099–1114.
14. Wehausen JV, Laitone EV. Surface waves. In *Encyclopedia of Physics*, Vol. 9. Springer-Verlag: Berlin, Germany, 1960; 446–778.
15. Dean RG, Dalrymple RA. *Water Wave Mechanics for Engineers and Scientists*. Prentice Hall: Englewood Cliffs, New Jersey, U.S.A., 1984.
16. Newman JN. Algorithms for the free-surface Green function. *Journal of Engineering Mathematics* 1985; **19**:57–67.
17. Teng B, Eatock Taylor R. New higher-order boundary element methods for wave diffraction/radiation. *Applied Ocean Research* 1995; **17**(2):71–77.
18. Ohmatsu S. On the irregular frequencies in the theory of oscillating bodies in a free surface. *Papers of Ship Research Institute* 1975; **48**:1–13.
19. Kleinman RE. On the mathematical theory of the motion of floating bodies - an update, 1982. DTNSRDC-82/074.
20. Lee CH, Newman JN, Zhu X. An extended boundary integral equation method for the removal of irregular frequency effects. *International Journal for Numerical Methods in Fluids* 1996; **23**(7):637–660.
21. Newman JN. Approximation of free-surface Green functions. In *Wave Asymptotics*, Martin PA, Wickham GR (eds). Cambridge University Press: Cambridge, United Kingdom, 1992; 107–135.
22. Telles JCF. A self-adaptive co-ordinate transformation for efficient numerical evaluation of general boundary element integrals. *International Journal for Numerical Methods in Engineering* 1987; **24**(5):959–973.
23. Lachat JC, Watson JO. Effective numerical treatment of boundary integral equations: a formulation for three-dimensional elastostatics. *International Journal for Numerical Methods in Engineering* 1976; **10**(5):991–1005.
24. Saad Y, Schultz MH. GMRES: a generalized minimal residual Algorithm for solving nonsymmetric linear systems. *SIAM Journal on Scientific and Statistical Computing* 1986; **7**:856–869.
25. Saad Y. A flexible inner-outer preconditioned GMRES algorithm. *SIAM Journal on Scientific and Statistical Computing* 1993; **14**(2):461–469.
26. Rokhlin V. Rapid solution of integral equations of classical potential theory. *Journal of Computational Physics* 1985; **60**(2):187–207.
27. Greengard L, Rokhlin V. A fast algorithm for particle simulations. *Journal of Computational Physics* 1987; **73**(2):325–348.
28. Newman JN. Wave effects on deformable bodies. *Applied Ocean Research* 1994; **16**(1):47–59.
29. Dvorkin EN, Bathe KJ. A continuum mechanics based four-node shell element for general non-linear analysis. *Engineering Computations* 1984; **1**(1):77–88.
30. Bathe KJ, Dvorkin EN. A formulation of general shell elements-the use of mixed interpolation of tensorial components. *International Journal for Numerical Methods in Engineering* 1986; **22**(3):697–722.
31. Lee PS, Bathe KJ. Development of MITC isotropic triangular shell finite elements. *Computers & Structures* 2004; **82**(11-12):945–962.

DOI: 10.1002/nme

32. Lee PS, Noh HC, Bathe KJ. Insight into 3-node triangular shell finite elements: the effects of element isotropy and mesh patterns. *Computers & Structures* 2007; **85**(7-8):404–418.
33. Lee PS, Bathe KJ. The quadratic MITC plate and MITC shell elements in plate bending. *Advances in Engineering Software* 2010; **41**(5):712–728.
34. Bathe KJ, Lee PS. Measuring the convergence behavior of shell analysis schemes. *Computers & Structures* 2011; **89**(3-4):285–301.
35. Lee Y, Yoon K, Lee PS. Improving the MITC3 shell finite element by using the Hellinger–Reissner principle. *Computers & Structures* 2012; **110–111**:93–106.
36. Yago K, Endo H. On the hydroelastic response of box-shaped floating structure with shallow draft (tank test with large scale model). *Journal-Society of Naval Architects of Japan* 1996; **180**:341–352.
37. Riggs HR, Niimi KM, Huang LL. Two benchmark problems for three-dimensional, linear hydroelasticity. *Journal of Offshore Mechanics and Arctic Engineering* 2007; **129**(3):149–157.

DOI: 10.1002/nme